Experimental and theoretical investigation of the role of nanofibrous topography feature size on adhesion of *Candida albicans*

Ah-Ram Kim

Thesis submitted to the faculty of the Virginia Polytechnic Institute and State University in partial fulfillment of the requirements for the degree of

Master of Science
In
Mechanical Engineering

Bahareh Behkam, Chair

Amrinder Nain

Rafael V. Davalos

February 27, 2015

Blacksburg, VA

Keywords: nanopatterned surfaces, biofilm, fungal infection, adhesion model, antifouling

Experimental and theoretical investigation of the role of nanofibrous topography feature size on adhesion of *Candida albicans*

Ah-Ram Kim

Abstract

Biofilm formation on medical devices is responsible for a substantial portion of healthcare associated infections with approximately 99,000 deaths and estimated financial burden of $28-$45 billion annually. Given the long-standing challenges of biofilm eradication, physical and chemical surface modifications to prevent biofilm formation from the early adhesion stage, continue to gain momentum.

Nanoscale structural features, ubiquitous in both natural and synthetic surfaces, are increasingly recognized to have wide-ranging effects on microorganism adhesion and biofilm development. In this thesis, bio-inspired nanofiber-coated polystyrene surfaces were developed to systematically investigate how highly ordered surface nanostructures (200nm-2000nm in size) impact adhesion and proliferation of model fungal pathogen, *Candida albicans*. A theoretical model for cell-textured surface interaction was also developed using thermodynamic principles to demonstrate that single cell adhesion to surface can be used to describe the population behavior. The trend for adhesion density of *C. albicans* on nanofiber-textured surfaces of varying diameters correlates with our theoretical finding of adherent single-cell energetic state.

Findings from this thesis can be used for enhanced *ab initio* design of antifouling surfaces for medical applications and beyond. We demonstrate a successful prototypical example of reduction in biofilm formation by optimally designed nanofiber coating of urinary catheters.

Acknowledgements

Foremost, I would like to thank my advisor Prof. Bahareh Behkam for all her guidance and support throughout not just my masters but also my undergraduate years. Over the past three years that I have worked with her, there were many times she had shown support not just professionally but also personally. I would not be where I am today without her support and belief in me to continue my studies as a graduate student. I also thank Prof. Amrinder Nain for all his support and contributions to my work. His generous guidance has helped greatly throughout my research experience. I would also like to thank Prof. Rafael Davalos for serving on my committee.

I want to thank my parents Jae-Yik Kim, and Won-Young Kim who always willingly sacrificed everything in order to support me. I would also like to thank my sister Mi-Song Kim for her support.

And of course, I would like to thank everyone from MicroN BASE laboratory including Aziz Traore, Ali Sahari, Zhou Ye, Chris Suh, Brian Geuther, Carmen Damico, Eric Leaman, and Peter Windes. Also, I want to thank all undergraduates that I have collaborated with including Evan Smith, Andrew Myers, and Jacquline Plyler. All members have provided so much support both with their friendship and intellectual guidance.

I would also like to thank members of the STEP lab including Kevin Sheets, Puja Sharma, Ji Wang, Amritpal Gill, Brian Koons, and Colin Ng. Also, I want to thank Tim O'Brien who first taught me how to spin fibers. I want to thank them all for their kindness and support and teaching me the STEP manufacturing method which has been an integral part of my research.

I would like to give special thanks to Emir Sahmanovic for helping me prepare for experiments, Dr. Karthik Nithyanandam for aiding me with optimization, and also Stephen McCartney for assisting me with SEM imaging.

I am also grateful for all the funding sources including Adhesion Society, Scieneering, Thomas F. and Kate Miller Jeffress Memorial Trust, and Mechanical Engineering start-up funds for Prof. Bahareh Behkam.

Lastly, I would like to thank all my friends and family who have seen my worst and the best throughout college and graduate school. I could not have come this far without all the support that helped me through it all.

Table of Contents

List of Figures

List of Tables

Chapter 1. Introduction

1.1 Adverse effects of microorganism adhesion

Colonization of microorganism of surfaces is known to have unfavorable effects in various fields such as aquatic flow systems and food industries. Its effect can also be detrimental in the world of medicine, especially with medical implants. The ability of microorganisms to infect indwelling devices is affiliated with their propensity to form biofilms. Biofilms are defined as structured communities of sessile cells embedded in extracellular polymeric matrix that are adherent to each other and the interface [1,2]. When microorganisms first encounter a surface, they adhere initially through non-specific interactions such as Van der Waals, electrostatic, or hydrophobic forces. This stage of adhesion also known as reversible adhesion takes place over a period of seconds. During the stage of irreversible adhesion which takes place over a period of minutes to hours, the microorganisms strongly adhere using their transmembrane receptor-ligand interaction. Subsequently, they begin to colonize and form a slimy biofilm which consists of extra-polymeric substance (EPS) such as polysaccharide and protein. When compared to the freely swimming planktonic cells, the sessile cells inside the EPS are more tolerant to antimicrobial stressors and human defense mechanisms [3]. Once biofilm has matured, clusters of cells detach from the matrix and the cycle of biofilm is repeated as shown in Figure 1.1.

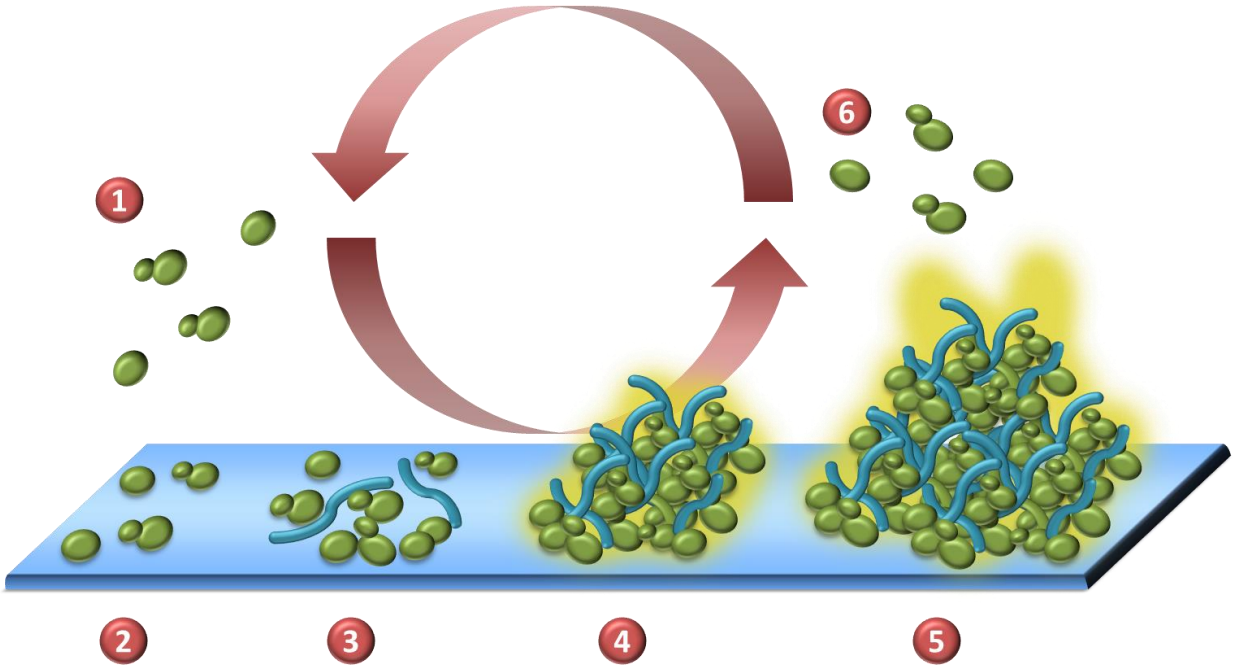

Figure 1.1. The stages of biofilm formation. 1) Planktonic cells that are freely moving around 2) attach to the substrate (reversible adhesion) and then adhere permanently to 3) replicate, differentiate, and form colonies. 4) The cells continue to grow and secrete extracellular polymeric substances (EPS) and encapsulate them in the matrix. 5) Once a mature biofilm is formed 6) some cells within the matrix are dispersed, repeating the biofilm development cycle. The circular shaped cells are the budding yeast cells (in green) and the elongated cells are the differentiated hyphae (in blue).

As a consequence of their resistance, it is virtually impossible to disinfect the medical devices once biofilm has formed on the surface. Current methods of treatment are long term antibiotics and surgical removal of the infected device both of which have many drawbacks. Long term antibiotic treatments are not very effective due to the protective nature of biofilm and can lead to further problems such as development of antimicrobial resistant strains [4]. Surgical removal can be costly and also because of the invasive nature, could be traumatic for patients especially since most with implanted devices are elderly. The estimated cost of medical and surgical treatment is

shown in Table 1.1 for initial device before replacement. Unfortunately, it is more likely for replacement implants to exceed in rate of infection by several folds [5].

Table 1.1. Average Rate of Infection and Cost Associated with Surgical Implants **[6].**

Implant	**Average Rate of Infection (%)**	**Estimated Average Cost of Both Medical and Surgical Treatment (US $)**
Mechanical heart valve	4	50,000
Vascular graft	4	40,000
Pacemaker – defibrillator	4	35,000
Ventricular assist device	40	50,000
Joint prosthesis	2	30,000
Fracture-fixation device	5	15,000
Ventricular shunt	6	50,000
Mammary implant	2	20,000
Penile implant	3	35,000

Biofilm is also responsible for healthcare-associated infections (HAIs) which are infections that develop in hospitals or health care environment that can affect both patients and hospital staffs. HAI is responsible for high mortality rates and economic loss. In 2002, there were approximately 99,000 deaths that were associated with HAI out of the 1.7 million HAI patients in the U.S. [7]. In 2007, the medical cost of HAI in U.S. hospitals range from $28.4 to $45 billion [8]. Because of these clinical and economic impacts of biofilm, novel methods of prevention or treatment are continuously sought.

Because adhesion of microorganism is seen as the starting point of biofilm formation and related infections, development of antimicrobial and anti-adhesion surfaces have been a subject of active research for many years [9,10]. The main objective of antibacterial or antimicrobial surfaces is to

either lyse or inhibit the growth of cells on the surface. Unlike antimicrobial surfaces, anti-adhesion surfaces simply prevent or delay the adhesion of cells to a surface. These two methods are used, individually or simultaneously so that formation of biofilm can be delayed, interrupted, or prevented.

1.2 State of the art antifouling surfaces

Antifouling surfaces can be made by altering the chemistry of the surface through anti-adhesive or intrinsically bioactive surface coatings [11]. Alteration of surface chemistries by adding surface-modifying end groups (SMEs) has been shown to reduce bacterial adhesion and biofilm formation [12]. Another approach is to coat the surface of biomaterials with materials known to have antimicrobial properties such as silver nanoparticles [13]. Although chemical treatment of surfaces and devices have been shown to reduce the activity of microorganisms *in vitro,* the inhibitory effect *in vivo* is known to only lasts up to 8 weeks due to the leaching of the chemical to the surrounding tissues [14]. Also, due to the presence of protein rich fluids inside the body, within seconds of placement of the devices, the protein adsorption to the surface reduce the antimicrobial properties.

Another chemical surface modification method reported is alteration to surface wetting properties to reduce cell adhesion. There have been reports of decrease in cell adhesion density of *C. albicans* with decreased hydrophobicity [12,15–18] but because of the different chemical compositions of the hydrophobic and hydrophilic materials, it is difficult to tell whether it is truly the hydrophobicity doing the work. Whether it is the different surface coatings, wetting properties, or chemical stimuli, change in chemical properties have dominated earlier surface modification techniques in preventing biofilm formation.

The effect of physical modifications to surface texture and stiffness or use of physical stimuli has been increasingly recognized as an alternative or complementary approach to the use of chemical stimuli. Although the idea of applying physical modification rather than chemical was unique, the results of earlier studies showed that by adding roughness to the surface, the adhesion was increased [19–22]. It was believed that roughness increases the surface area and thus the possible adhesion sites for the microorganisms. Contradicting previous beliefs, recent advancements of techniques in fabricating nano/micropatterns proposed state-of-the-art biomimicking surfaces [23] that have antifouling effects without any influence from the chemistry of the surface. Micropatterns such as pillars that mimic shark skin [24] are used as physical obstacle for the expanding colonies of microorganisms. Nanopatterns such as lotus-leaf-like superhydrophobic surface [25] and cicada wing surface [26] have been proven to show reduction of microorganism adhesion and cell lysing by puncturing of microbial membrane, respectively.

1.3 *Candida albicans*

One of the most common and important human fungal pathogens is the *Candida albicans.* This opportunistic pathogen grows in various morphologies. There is the budding yeast form which is spherical in morphology and can vary in diameter from 2 to 8 μm. There is also the elongated filamentous hypha which is approximately 2 μm in diameter and can vary in length. The phenotypic switching is induced by various environmental conditions such as temperature, pH, or culturing media [27]. In a typical *C. albicans* biofilm, a mixture of yeast and filamentous forms are networked together. The dimorphism in *C. albicans* is important because hyphal form of the fungal cell is hypothesized to be a virulent factor. *In vitro* studies show that filamentous forms invade the agar substratum which lead to the conclusion that it may be important for penetrating to bloodstreams and colonizing inside organs *in vivo* [27,28]. Furthermore, the

mechanical force along with protease and phospholipase activity at the hyphal tip was observed during studies of tissue invasion [28]. Another virulence factor *C. albicans* is adhesion. Similarly to most other microorganisms, *C. albicans* have the ability to adhere to surfaces, forming infection causing biofilms. The adhesion is mediated by adhesins, or biomolecules that promote adherence to surface ligands [29].

C. albicans are notorious for their versatility characterized by the ability to survive and cause diseases in different anatomical sites of the host [29]. It also possesses the ability to infect medical devices such as in-dwelling catheters, prosthetic joints, heart valves, and more [30]. The pathogenic yeast is responsible for high mortality rates and increase in costs of care and duration of hospitalization for growing number of immunocompromised patients and those who use indwelling medical devices [31]. Candidiasis is the fourth leading cause of nosocomial infection in the United States with high mortality rates of up to 60% [32].

1.4 Motivation

A previous study by our group showed that various microbial adhesion modes and density outcomes result from varying feature size and spacing of surface topographical features. Nanofibrous surface texturizing inspired by anti-fouling topography of *Mytilus edulis*, also known as mussel, was utilized to study the effects of topography on *Pseudomonas aeruginosa* adhesion. By varying feature size and spacing (fiber diameter: 91-971 nm, fiber edge-to edge spacing: 300-1800 nm), it was found that aligned fibers with diameters similar to the bacteria diameter and fiber separation distance less than the bacteria diameter showed lower adhesion density by minimizing the contact area the cell has with the surface [33]. The results of this unique fibrous patterning have prompted us to create submicron fibrous topographic features on

biomaterial surfaces to investigate adhesion and biofilm formation behavior of *Candida albicans*, a model fungal pathogen, in order to develop surface engineering strategies for preventing the biofilm development process.

1.5 Objectives and Organization of the Thesis

Motivated by urgent need for a method of preventing fungal biofilm formation, our study is prompted with the goal of using surface engineering methods to develop a general framework for antifouling surface design. Our focus is on investigating the *C. albicans* adhesion behavior on aligned nanofibrous topography of various feature sizes. We hypothesize that eukaryotic fungal cell will also follow the previously seen trend with bacterial cells, specifically *Pseudomonas aeruginosa* [33] and that we can use the energetic state of a single cell-fiber interaction to explain the population level adhesion behavior seen in the experimental results. The remainder of this thesis is organized as follows:

Chapter 2: This chapter details the experimental approach for construction and characterization of nanofiber coated surfaces and for study of *C. albicans* adhesion and metabolic activity on the aforementioned engineered surfaces. Materials and methods used to conduct the assays of quantifying the cell number and cell metabolism activity are included in this chapter along with the results. The results include the trend in cell adhesion density and metabolic activity on surfaces as a function of nanofiber diameters. Also, two different catheter materials were tested to see if adhesion reduction trend observed on flat substrates will also be true on three dimensional non-planar substrates.

Chapter 3: This chapter introduces a thermodynamic model which describes the adhesion behavior at a single cell level. The model is based on the thermodynamic principle that cells

adhere to surfaces such that their overall free energy is minimized. We examined the effect of substrate topography-induced deformation on overall energy gain and expenditure. Similar to Chapter 2, the effect of fiber diameter on the total free energy of the cells was investigated.

Chapter 4: This chapter includes the results of the experimental and theoretical work detailed in the previous two chapters and a detailed discussion on the correlation between the two bodies of work. Also, a modified theoretical model based on the differentiated morphology of the cell is introduced to discuss the possible variation in the adhesion behavior. This chapter also includes a statistical analysis of the experimental data, carried out by grouping the diameters and looking for the significant differences in the cell numbers for each of the groups. This chapter is concluded with a summary of the findings, a discussion on the original contributions of this thesis and its potential impact on the field of antifouling surface design, and possible future directions.

Chapter 2. Experimental approach for surface modification and study of *C. albicans* adhesion

This chapter examines the effect of surface nanotopographies in form of nanofibers on the adhesion of *C. albicans.* The surface modification technique used to create highly aligned polystyrene nanofiber coating of controlled diameter and separation distances on polystyrene surface and the experimental approach used for dynamic adhesion assay are discussed along with methods of analysis and results.

2.1 Materials and Methods

2.1.1 Yeast Strain

Wild-type *Candida albicans* strain SC5314 (ATCC MYA2876, American Type Culture Center, Manassas, VA) was used throughout the study. The protocol for preparation of the microorganism by Chandra *et al.* [34] was followed. The frozen stock cultures were stored in -80 ℃. Using an inoculating loop, *C. albicans* was streaked onto the sabouraud dextrose agar (SDA, Beckton Dicknson, Franklin Lakes, NJ) plate and incubated at 37 ℃ for 16-24 hours. Subsequently, 3-5 single cell colonies were inoculated into 10 ml of yeast nitrogen base (Beckton Dicknson, Franklin Lakes, NJ) with 50 mM dextrose (Fisher Scientific, Pittsburgh, PA) (YNBD) inside a sterile 50-ml polypropylene tube. The inoculated tube was then put on a shaking incubator at 37 ℃ and 150 rpm for 20-24 hours.

2.1.2 Nano-textured surface fabrication

A 0.125 mm polystyrene (PS) sheet (Goodfellow Cambridge Ltd., Huntington, England) was cut into 3 mm×15 mm rectangular pieces. The polystyrene substrates were washed with 100%

ethanol and rinsed with deionized (DI) water before the deposition of surface texture. The smooth polystyrene substrate (mean roughness = 1.24 nm) without nanofibrous texture was used as control surface for the experiment.

For texturizing the surface, the non-electrospinning Spinneret based Tunable Engineered Parameters (STEP) method was utilized (Figure 2.1) [35]. In this pseudo-dry spinning process, polystyrene (molecular weight: 2×10^6 g/mol, Scientific Polymer Products, Ontario, NY) dissolved in xylene was pumped through a glass microneedle mounted on a manual precision XYZ positioning stage. A continuous fiber, extruded from the polymer solution droplet at the tip of the microneedle, was deposited onto a rotating polystyrene substrate which was mounted onto a stepper motor (208 Compact Stepper motor, Lin Engineering, Morgan Hill, CA) attached to a motorized XYZ positioning stage. The rotational speed of the motor and the translational speed of the stage determine the edge-to-edge spacing between the fibers. This method allows for highly aligned polystyrene nanofibers with controlled diameter and spacing to be deposited onto the polystyrene substrate. The diameter was controlled by changing the diameter of the microneedle and the concentration and molecular weight of the polymer in the polystyrene-xylene solution. The polystyrene was dissolved in xylene at 10-25% by weight to achieve fiber diameters in the range of 250-2000 nm. For all the diameters, the edge-to-edge separation distance between the fibers was kept constant at approximately 2000 nm. In order to keep the spacing constant between different diameter samples, the linear velocity of the motorized stage was varied when spinning each of the diameters.

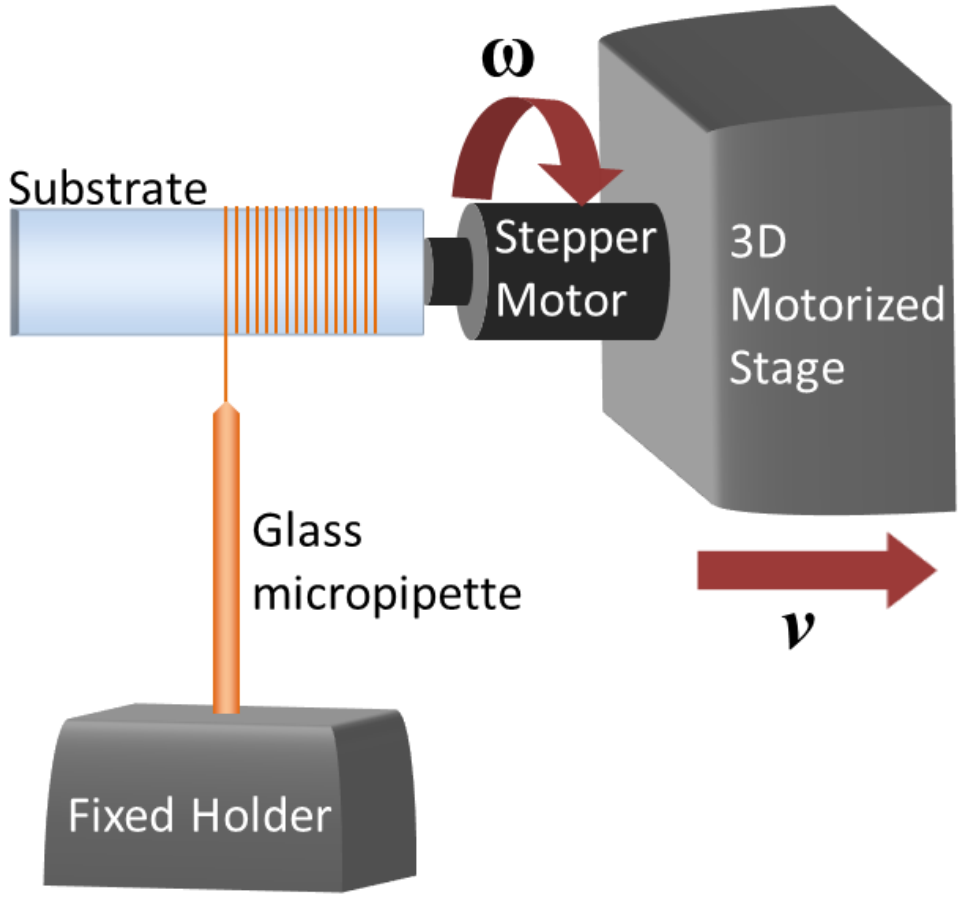

Figure 2.1. STEP fiber manufacturing platform used to construct nanofiber textured substrates. The 3D motorized stage moves linearly with velocity *v* while stepper motor rotates the substrate at rotational velocity of ω. As the substrate moves, it pulls and collects the polymeric solution from the glass micropipette that is continuously pumping the solution.

For the catheter experiments, latex (Bard Medical, Covington, GA) and silicone (Rochester Medical, Stewartville, MN) catheters with diameter of 4.7 mm and length of 15 mm were used as substrates on which 900~1000 nm diameter fibers were deposited at the edge to edge separation distance of 2000 nm. Smooth (uncoated) catheters were used as controls for the experiments.

Prior to all experiments, the diameter and separation distances of the fibers were analyzed using Environmental Scanning Electron Microscope (ESEM) (FEI Quanta 600 FEG, Hillsboro, OR) in

in low vacuum mode. Ten random areas (magnification: 8000x) along the horizontal centerline of the fibrous samples were imaged. Measurements of the diameter and separation distances were done using image analysis software ImageJ.

2.1.3 Dynamic retention assay

All retention assays were performed in a Center for Disease Control (CDC) biofilm reactor (Model CBR-90-2). The CDC biofilm reactor (Figure 2.2a) consists of a 1 L glass vessel with eight polypropylene rods. The baffled stirrer is located in the center of the vessel, perpendicular to the rods, providing a constant shear flow across the surface of the rods, where the nanofiber-textured surface were mounted (Figure 2.2.b). The dynamic assay was conducted according to the methods previously established by Chandra *et al.* [34]. The nanofiber-coated polystyrene substrates were sterilized under ultraviolet light inside a biological safety cabinet for 45 minutes and conditioned by soaking in fetal bovine serum for 8-12 hours prior to the experiment. The substrates were then mounted onto the bioreactor rods using polydimethylsiloxane (PDMS, SYLGARD® 184 silicone elastomer, Dow Corning, Midland, MI) as adhesive. The silicone elastomer was mixed at a ratio of 10 parts base to 1 part curing agent and cured in a petri dish on a hot plate at 85 ℃ for 6 to 7 minutes until the PDMS reached glue consistency. The polystyrene samples were placed onto the rods so that the direction of the fibers is vertical and perpendicular to the shear (Figure 2.2b). Each rod held triplicate samples of the same fiber diameter.

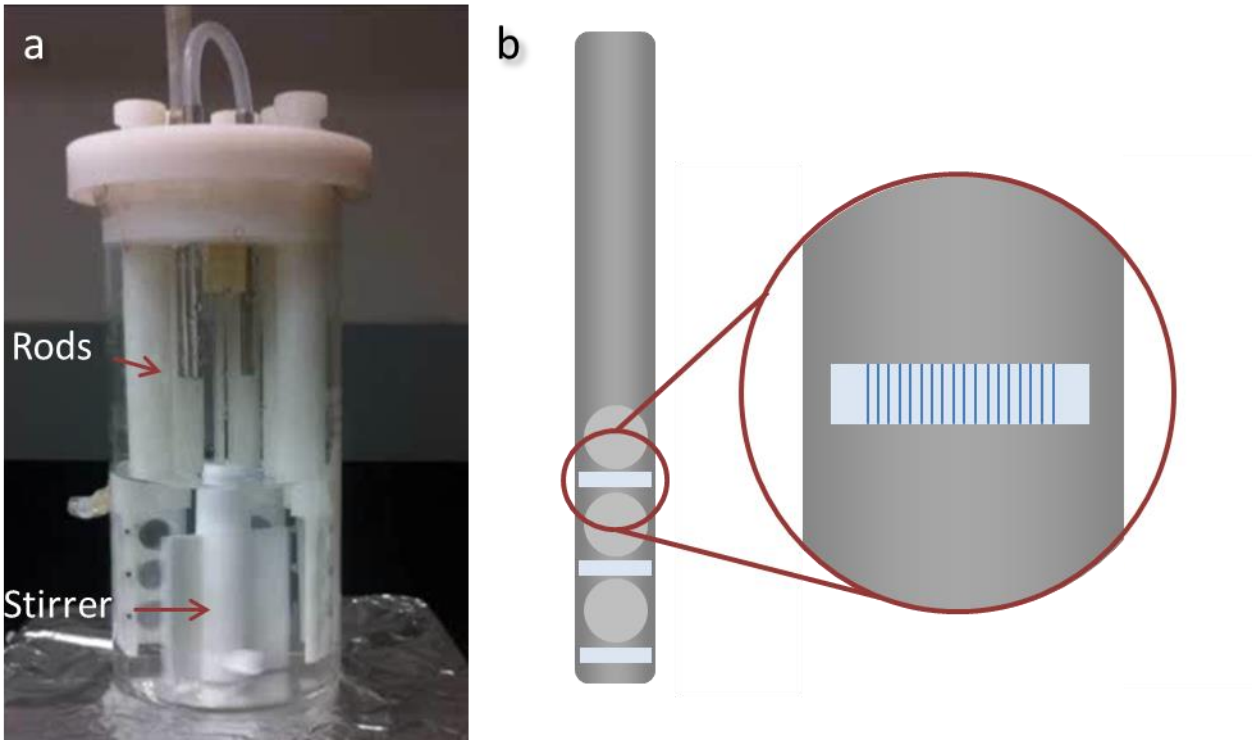

Figure 2.2. a) Center for Disease Control (CDC) biofilm reactor showing the rods and baffled stirrer inside the vessel. b) The illustration of a rod with close-up of the mounted sample, showing the fiber direction which is perpendicular to the shear.

The *C. albicans* culture was adjusted to an optical density OD_{520} of 0.385 which corresponds to 1×10^7 cfu/ml [20]. Subsequently, 8 ml of cultured cells were added to 392 ml of YNBD to makeup a total of 400 ml of culture inside the CDC biofilm reactor. Then, the reactor was placed on a magnetic stir plate inside an incubator at 80 rpm and 37 ℃, mimicking physiological shear and temperature, for 24 hours. Same retention assay was performed for the catheters.

2.1.4 Quantification analysis

2.1.4.1 Colony counting preparation

The rods were carefully removed from the CDC reactor and the substrate samples were removed using a pair of fine tipped tweezers. Each sample was placed inside a petri dish (Fisher Scientific, Pittsburg, PA) and cells on 2 mm × 2 mm area on each ends of the samples were removed by scraping with wooden toothpicks. The scraped areas were left uncoated for sample mounting and handling purposes. The sample was then washed by addition of 4 ml of phosphate buffered saline (PBS, Mediatech, Manassas, VA), followed by light swirling and aspiration of the solution.

2.1.4.2 Colony counting analysis

The samples used for colony counting analysis were each placed inside a 15 ml polypropylene test tubes (Fisher Scientific, Pittsburg, PA), containing 10 ml of sabouraud dextrose broth (SDB, Beckton Dicknson, Franklin Lakes, NJ). The cells adhered to the samples were removed by consecutive sonication (Branson 1510, 42 kHz, 70 W, Branson Ultrasonics, Danbury, CT) and vortex mixing at 1000 rpm (Fisher Scientific, Pittsburg, PA), for 30 seconds each, repeated three times [36]. The resulting cell suspension was serially diluted by a factor of 100 in SDB and a 100 µl aliquot from the final dilution was pipetted onto SDA and spread with sterilized cell spreaders (Bel-Art, Wayne, NJ, USA). The finished plates were incubated at 37 ℃ for 24 hours and the number of visible colonies was counted. Same washing procedure and colony counting analysis was performed for the catheters.

The results from the nanofiber-textured samples were compared to the bare (uncoated control) from the same experiment by taking the ratio of the number of cells on the nanofiber-coated surface of each diameter and dividing it by the number of cells on the surface of the bare from the same experiment. This makes the ratio on bare surface equal to 1 and anything below 1

indicated decrease in the adhesion of cells (relative to the bare control) and anything above indicates increase.

2.1.4.3 XTT analysis

The nanofiber-coated samples used for XTT analysis were transferred from the bioreactor into a 12-well-plate (Corning Life Sciences, Tewksbury, MA). Each sample was put in a single well with 2 ml of PBS, 50 µl of 2 mg/ml XTT solution (Sigma-Aldrich, St. Louis, MO), and 4 µl of 2 mM menadione solution (Sigma-Aldrich, St. Louis, MO). The well-plate was covered with aluminum foil to avoid exposure to light and was placed inside a 37 ℃ incubator or 5 hours. The contents were then transferred to a 15 ml tube and centrifuged for 5 minutes at 3000×g. The optical density of the supernatant was measured with a UV/vis spectrophotometer (Cary 60 UV-Vis, Agilent Technologies, Santa Clara, CA) at 492 nm. The spectrophotometer readings were normalized with respect to the bare surface from the same experiment, similar to the approach described in 2.1.4.2.

2.1.5 Imaging

Fixed SEM was carried out with all samples fixed in 2.5% glutaraldehyde at 4 ℃ and dehydrated through series of ethanol washing at room temperature. The samples were imaged using an ESEM system under high vacuum mode.

Live SEM was done on the same day the retention assay was completed within hours of removal of the sample from the bioreactor. The samples were transferred from the bioreactor into a PBS containing well-plate and carried to the microscopy facility then were image using an ESEM system operated under the low vacuum mode (Figure 3.2).

2.1.6 Statistical analysis

Significant differences of the groups were determined using JMP software (SAS, Drive Cary, NC, USA). The means of each group of diameters were compared using Tukey's HSD test with alpha value of 0.05 to determine statistical significance (Figure 4.6).

2.2 Results

2.2.1 Nanofibrous surface texturing

Using STEP technique, aligned PS fibers with diameters varying between 200 nm to 2000 nm were deposited onto PS substrates with edge-to-edge separation distance of approximately 2 μm (Figure 2.3). Table 2.1 shows the polymer molecular weight, solution concentration, and microneedle diameter for each of the fiber diameters. The measurement of all the fiber diameters (Figure 2.4) and separation distances (Figure 2.5) for all samples used for analysis were plotted as histograms to show the distribution. As the PS solution concentration increases, the variability of the fiber diameter increases, with range of resulting diameters widening. However, the edge-to-edge spacing of the fibers remains constantly near 2000 nm due to the varied linear velocity during the spinning processes. By increasing the linear velocity for more concentrated PS solutions (used for making larger diameter), the spacing can be kept constant throughout samples with varying diameters. After imaging and analysis, only samples with uniform spacing and diameters were utilized in the experiments.

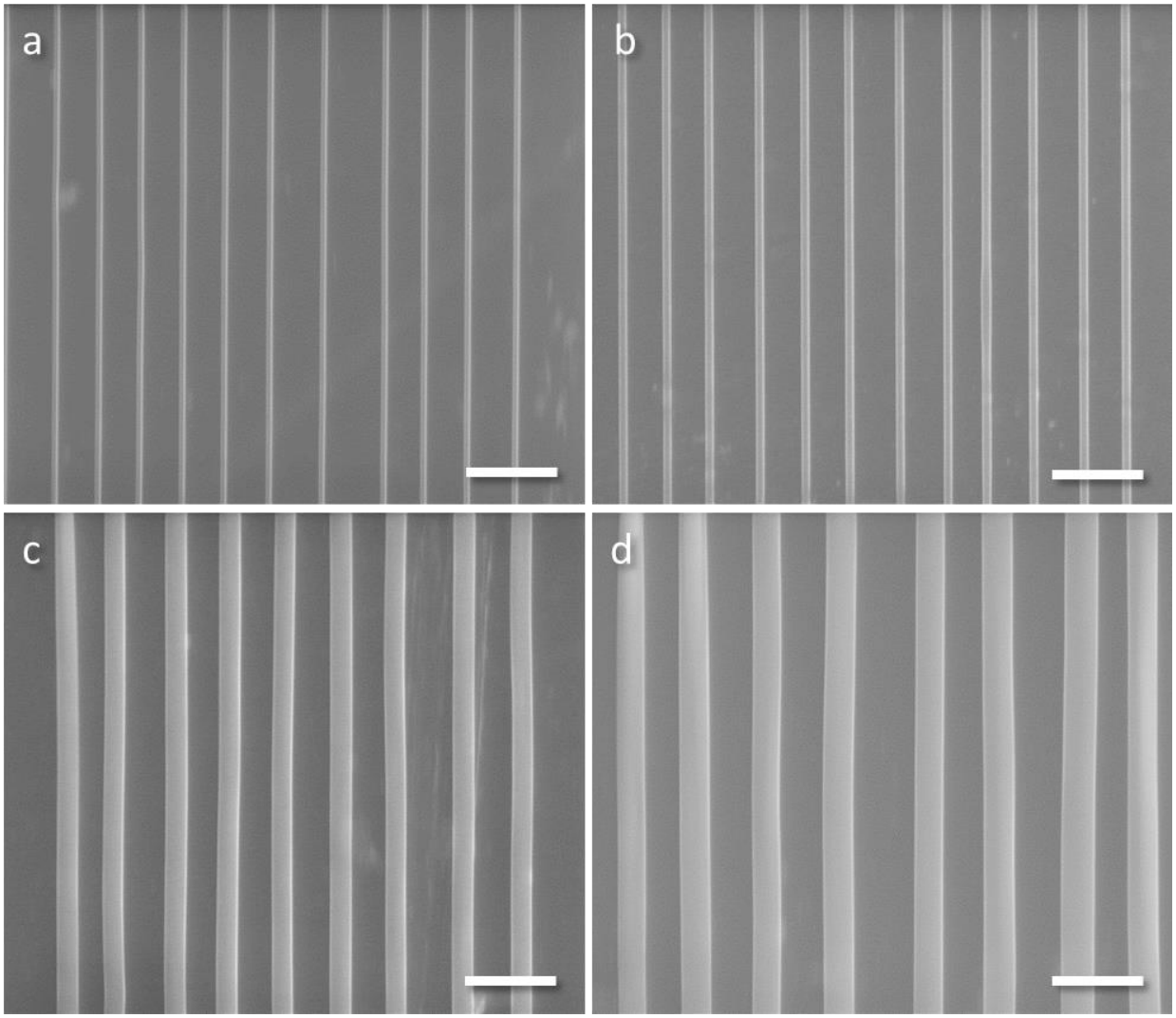

Figure 2.3. Electron micrograph of nanofibers manufactured with various PS solution concentration resulting in different diameters of (a) 300 nm, (b) 500 nm, (c) 1000 nm, and (d) 1600 nm. The scale bar represents 5 μm.

Table 2.1. Solution concentration and glass needle diameter and the corresponding fiber diameter range.

Solution concentration‡ (%)	**Glass Needle Diameter (µm)**	**Sample Average Fiber Diameter (nm)**	**Standard Deviation (nm)**
10	20	362	119
14	30	609	141
16	35	1103	284
18	40	1232	356
20	45	1488	334
22	50	1810	360
25	55	2039	448

‡ For all solutions, polystyrene with molecular weight of 2×10^6 g/mol was dissolved in xylene (w/w).

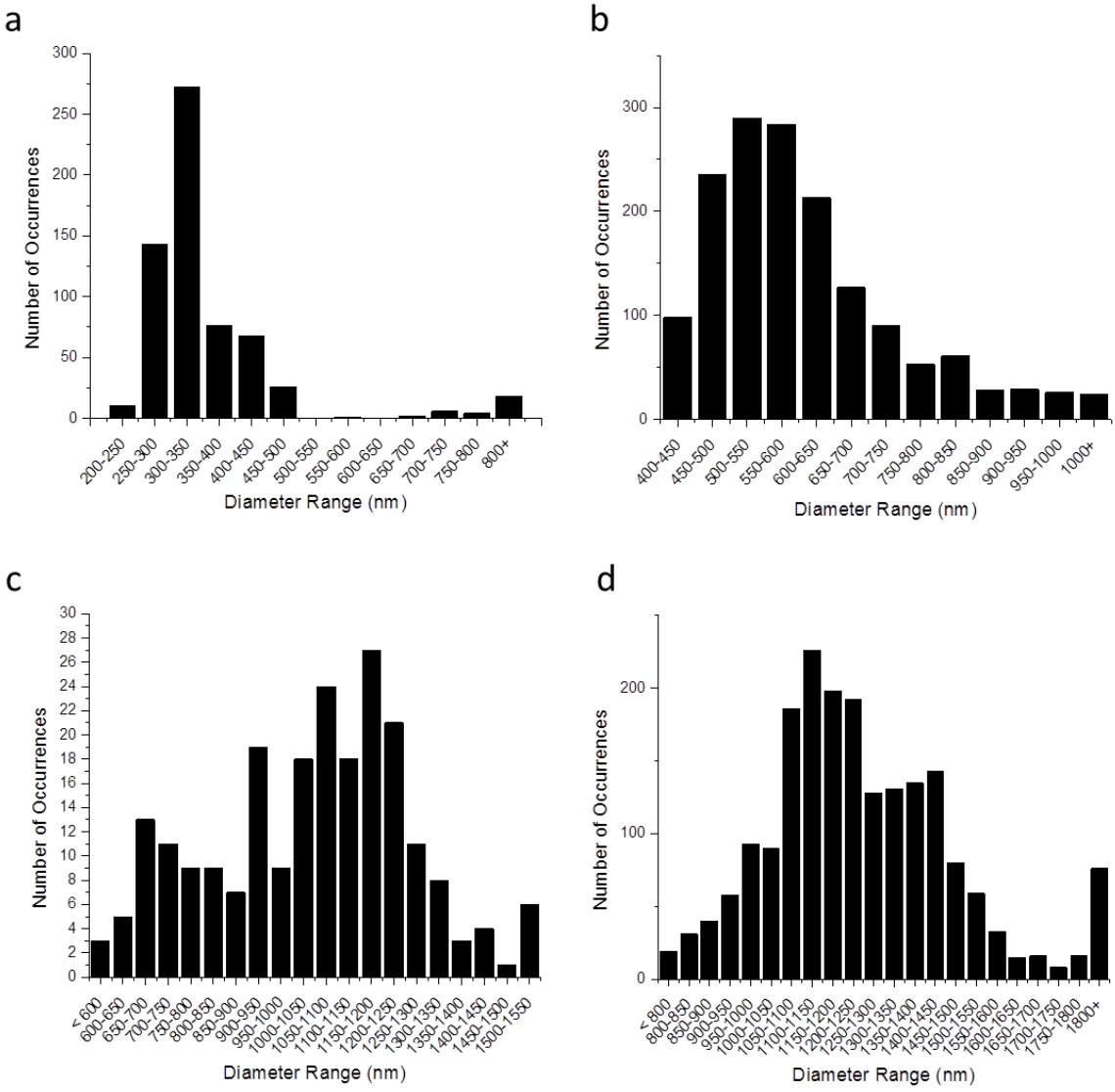
a
Number of Occurrences
Diameter Range (nm)
b
Number of Occurrences
Diameter Range (nm)
c
Number of Occurrences
Diameter Range (nm)
d
Number of Occurrences
Diameter Range (nm)

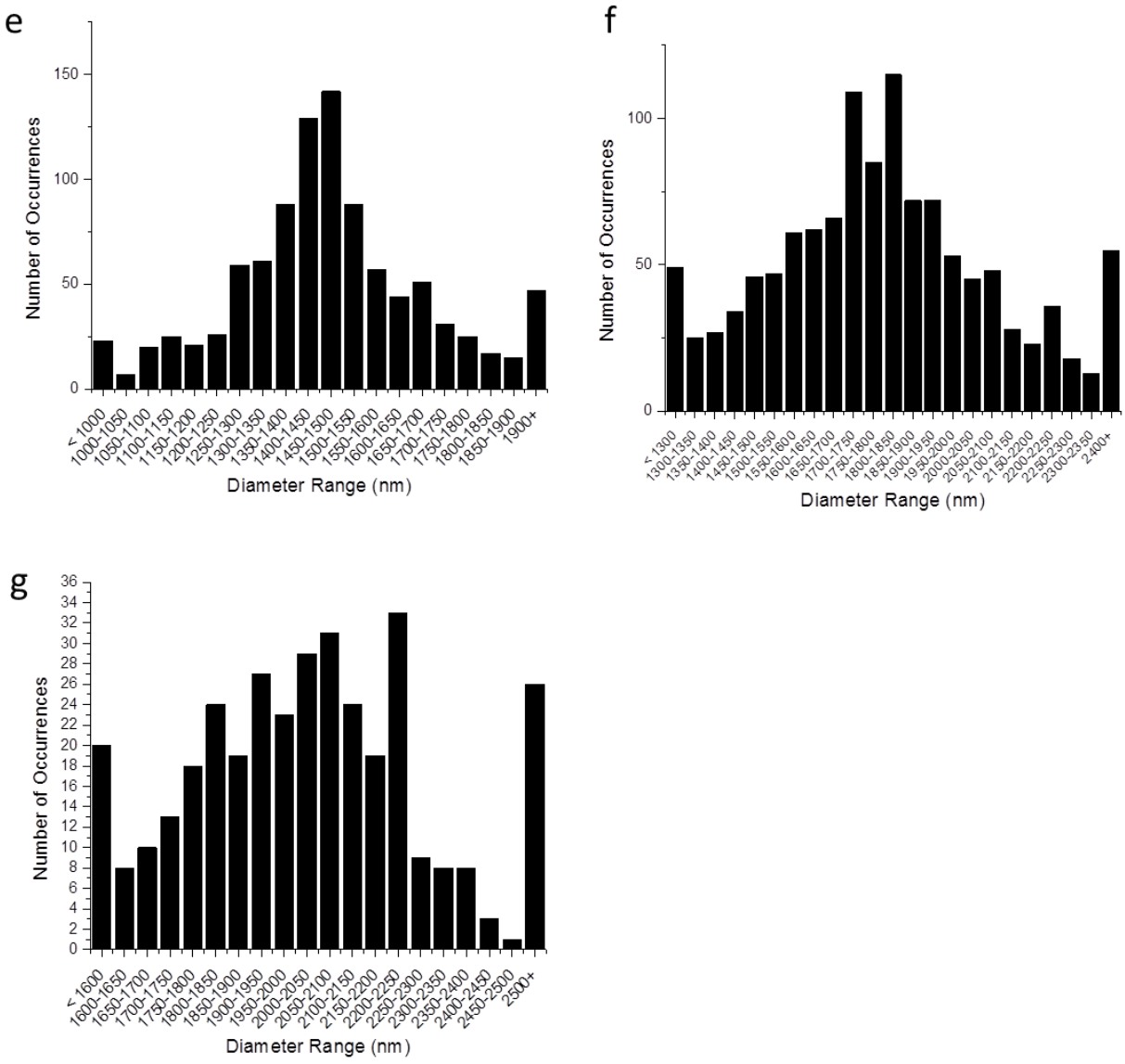

Figure 2.4. Histograms of fiber diameters STEP manufactured from (a) 10% (b) 14% (c) 16% (d) 18% (e) 20% (f) 22% and (g) 25% (w/w) PS solution in xylene.

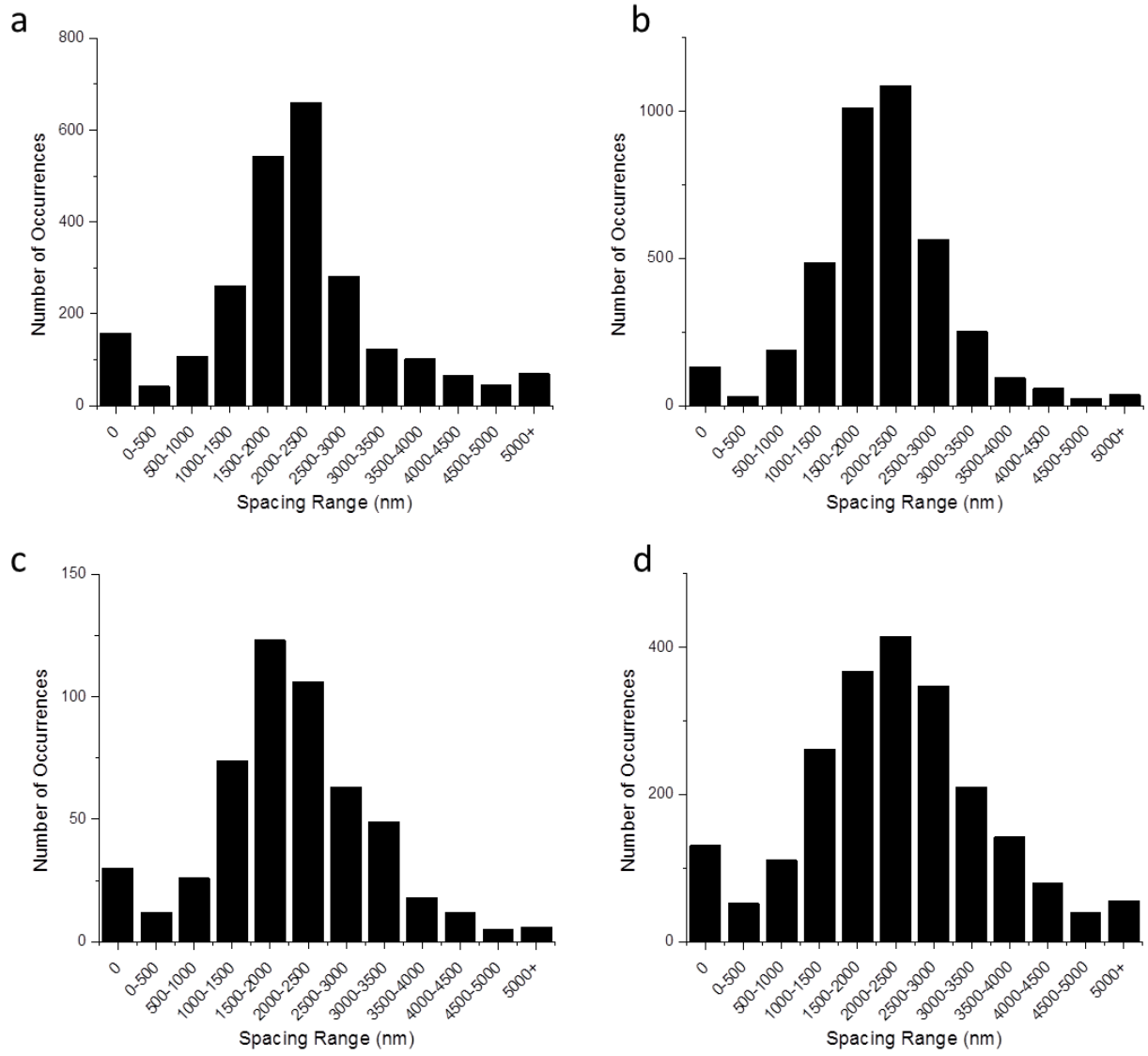
a
Number of Occurrences
800
600
400
200
0
0
0-500
500-1000
1000-1500
1500-2000
2000-2500
2500-3000
3000-3500
3500-4000
4000-4500
4500-5000
5000+
Spacing Range (nm)
b
Number of Occurrences
1000
500
0
0
0-500
500-1000
1000-1500
1500-2000
2000-2500
2500-3000
3000-3500
3500-4000
4000-4500
4500-5000
5000+
Spacing Range (nm)
c
Number of Occurrences
150
100
50
0
0
0-500
500-1000
1000-1500
1500-2000
2000-2500
2500-3000
3000-3500
3500-4000
4000-4500
4500-5000
5000+
Spacing Range (nm)
d
Number of Occurrences
400
200
0
0
0-500
500-1000
1000-1500
1500-2000
2000-2500
2500-3000
3000-3500
3500-4000
4000-4500
4500-5000
5000+
Spacing Range (nm)

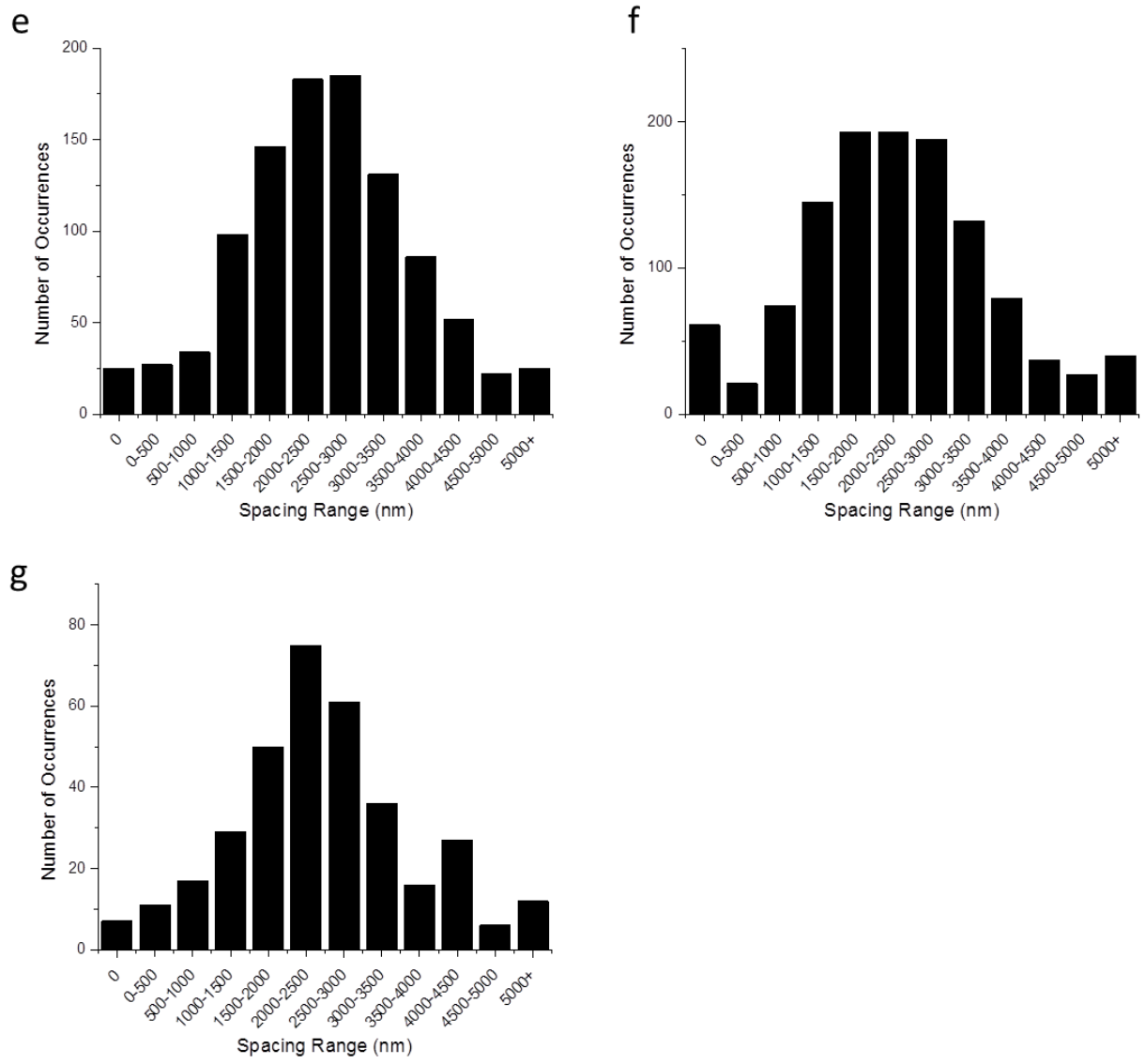

Figure 2.5. Histograms of the spacing (edge-to-edge separation distance) of STEP manufactured fibers from (a) 10% (b) 14% (c) 16% (d) 18% (e) 20% (f) 22% and (g) 25% (w/w) PS solution in xylene.

2.2.2 Cell adhesion quantification

C. albicans adhesion to surface was primarily characterized by methods of serial dilution and colony counting. Secondary analysis was done using XTT method which quantifies the metabolic activity of the cells and was used to confirm the trend observed in the colony counting assay. Figure 2.6a shows the normalized cell number for various fiber diameters and a "U-shaped" trend is clearly visible with minimum adhesion at diameters of 1000-1400 nm. This "U-shaped" trend is created by the high density of cells at both small and large ranges of the fiber diameters and lower density of cells in the middle range fiber diameters. The XTT results (Figure 2.6b) indicate similar trend and have minimum adhesion around 1000 nm, supporting the results from colony counting method. The cell attachment on smooth and nanofiber-coated substrates of various diameters is shown in Figure 2.7. It can be seen that with increase in cell density, hyphal formation is also increased.

To investigate the applicability of our findings to 3 dimensional substrate, retention assay and colony counting was performed on latex and silicone catheters (Figure 2.8). For latex catheters, the nanofiber coating resulted in a 40% reduction in cell adhesion, while the reduction on the silicone catheter was limited to only 10%.

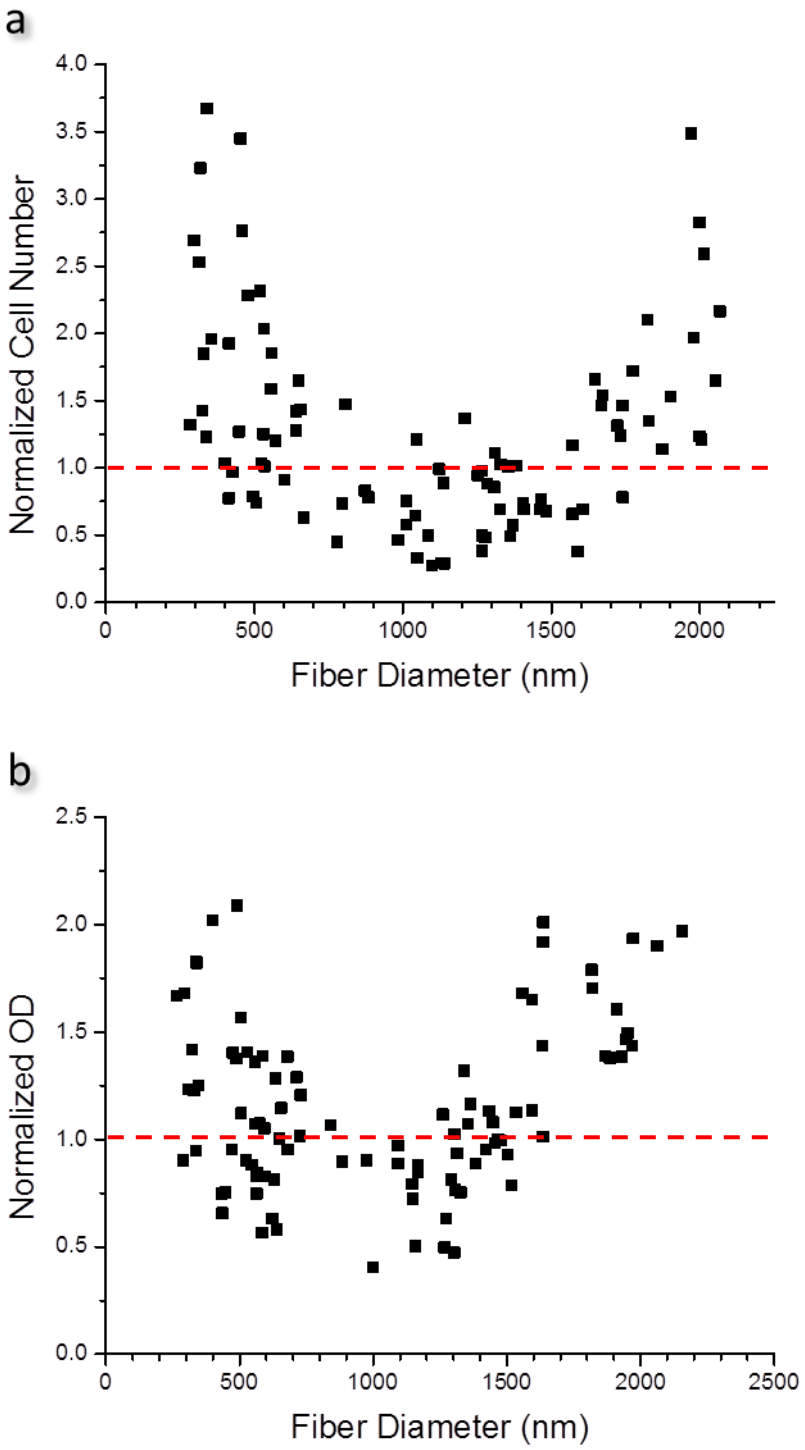

Figure 2.6. The normalized (a) cell numbers from colony counting (n=94) and (b) optical density (OD) from XTT analyses (n=96). Data in both plots are normalized with respect to uncoated control surfaces (shown as red dotted lines). A single data point on the plot represents a single sample.

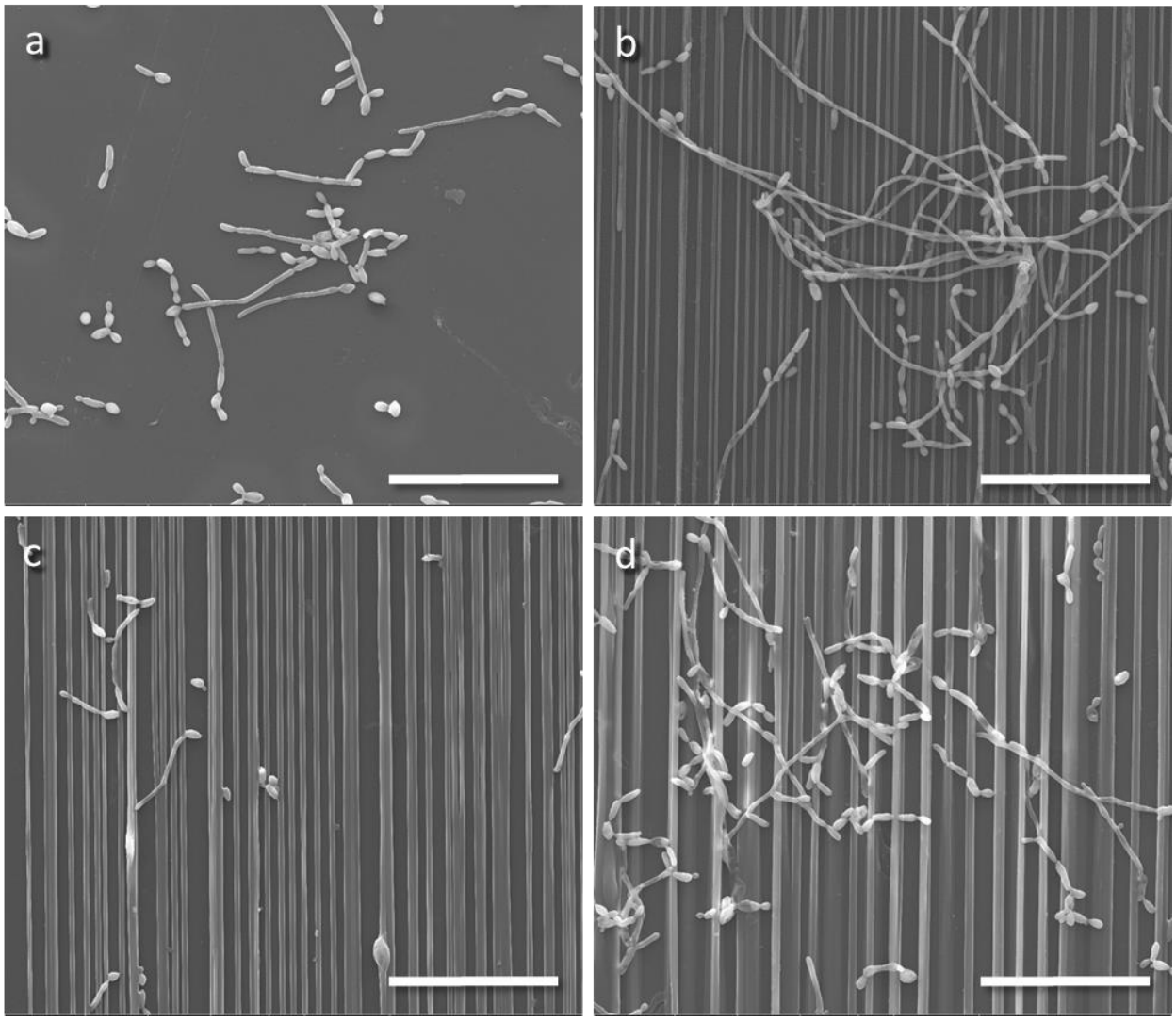

Figure 2.7. Cell attachment on (a) bare, (b) 300 nm, (c) 1000 nm, and (d) 2000 nm fiber-coated substrates after a 24 hour adhesion assay. All scale bar represent 50 μm.

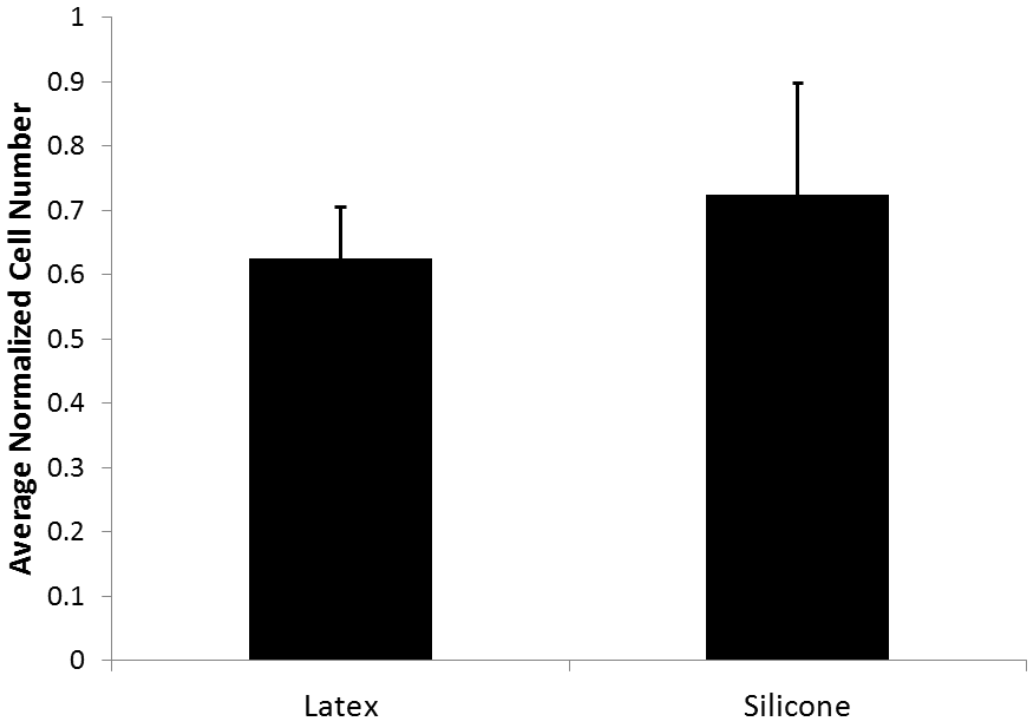

Figure 2.8. The average normalized cell density on latex (n=4) and silicone catheters (n=4). The density on fibrous catheter was normalized to the density on bare catheter of the same material.

2.3 Discussion and Conclusions

STEP method was used to create 200-2000 nm diameter fiber-coated surfaces at constant edge to edge spacing to investigate the role of surface topography in *C. albicans* biofilm development. Our results show that *C. albicans* adhesion density follows a "U-shaped" trend in both colony counting and XTT assays. This "U-shape" is caused by the increased densities in small and large diameter fiber samples and decreased density in the middle diameter fiber samples. Our results indicate that by simply altering the surface topography, the adhesion density of yeast onto the substrate can be reduced to as little as 20% or increased to as high as 400% when compared to the smooth surface (uncoated). The experiment was repeated on 3-dimensional cylindrical catheters of two materials-latex and silicone. The results of the catheter experiments show that

the results observed on 2-dimensional surfaces are preserved and addition of surface coating can reduce adhesion of *C. albicans* by as much 30%. This shows the feasibility and versatility of using STEP-based surface coating methods for medical implant or indwelling devices.

Chapter 3. Adhesion Model

In this chapter, an analytical model for single cell adhesion on nanofiber-textured surfaces is developed. We aim to investigate the relationship between the total free energy of a single adherent cell and adhesion density of the cell population that was quantified in the previous chapter. The energetic state of the single cell is described by the thermodynamic principals of net balance of energy gain and energy expenditure.

Nomenclature

a	Fiber radius
A	Adhesion energy density
D_f	Fiber separation distance
L	Hyphal length
n	number of fibers cell interacts with
E_{ad}	Adhesion energy
E_{adf}	Fiber adhesion energy
E_{ads}	Substrate adhesion energy
E_c	Curvature energy
E_{el}	Elastic energy
E_{tot}	Total energy
k_a	Modulus of elasticity
k_c	Modulus of curvature
R_0	Initial cell radius
R	Cell radius after adhesion
S_0	Initial cell surface area

S	Cell surface area after adhesion
S_{ad}	Total apparent contact area
$\underline{S_{sub}}$	Cell-substrate contact area
S_{fiber}	Cell-fiber contact area
S_T	Surface area of curvature portion
z	Degree of penetration
α	Angle between fiber and toroid cross-sections
β	Angle between centerlines of cell-toroid and cell-fiber
δ	Distance between toroid and fiber centerlines
ϵ	Relative excess surface area of the cell
θ	Cell-substrate contact area contact angle
ρ	Curvature radius

3.1 Model

3.1.1 Net free energy

The total free energy (E_{tot}) results from the net balance of the energy gain and energy expenditure in the process of adhesion. At the cell-surface interface, as energy gain decreases and/or energy cost increases; it becomes thermodynamically unfavorable for the cells to adhere at a site. In previous work from our lab [33] and others [37], early stage adhesion of microorganisms to micro/nano-textured surfaces was qualitatively discussed using thermodynamics principles underlying interaction between a vesicle and a rigid surface. During the past few years, the vesicle-rigid body interaction mathematical models [38,39], have been shown to effectively describe thermodynamics of biological adhesion [26,40]. The previous models have been developed for vesicle wrapping of small spherical particles, looking at both

partially and fully enveloped cases depending on different combinations of ratio of particle and vesicle size, stretching, and bending moduli of the membrane. In this chapter, we built upon the previous work and developed a mathematical model that describes the interactions between *Candida albicans* (in both yeast and hyphal form) and the nanofiber-textured substrates, including both interactions with the fibers and the underlying substrate.

The cross sectional geometry of the cell-fiber interface, shown in Figure 3.1a, demonstrates localized deformation of the cell, valid for both yeast and hyphal forms. The dimensionless parameter, z, represents the extent to which the cell wraps around the fiber. The two radii δ and ρ are used to define the geometry of the two cylinder-like segments of the deformed cells. The cell shape at adhesion is assumed as shown in Figure 3.1b. To support our assumptions, live SEM of *C. albicans* were taken to observe the membrane morphology of the adherent cells. The SEM was taken of the live cells rather than fixed in order to preserve the natural membrane properties since dehydrated membrane may take other forms other than that prior to fixing. Figure 3.2a, and b show the *C. albicans* attachment on small diameter fiber (~300 nm). It is visible that the cell membrane wraps deeply around the fiber and that the cell deformation is very local, not effecting the overall shape of the cell. However, with bigger diameter fibers (~1800 nm) in Figure 3.2c and d, the cell only partially wrap around the fiber and do not contact the underlying substrate. The partial wrapping of the cell and the associated deformation seems to take place over the entire cell membrane rather than just locally.

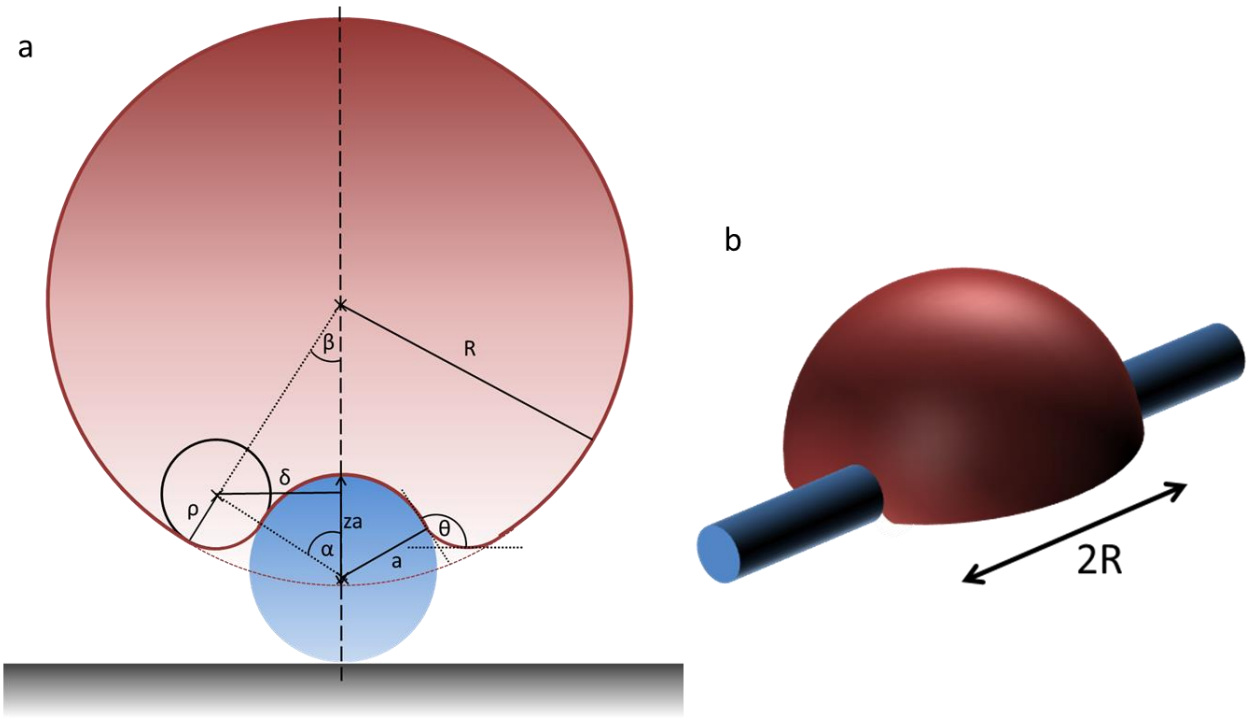

Figure 3.1. (a) A two-dimensional cross-section view of cell (red) adhering to the fiber (blue) on substrate (gray). Partial wrapping (no contact with the flat substrate) is shown. (b) The 3 dimensional depiction of the cell shape at adhesion with fiber and substrate.

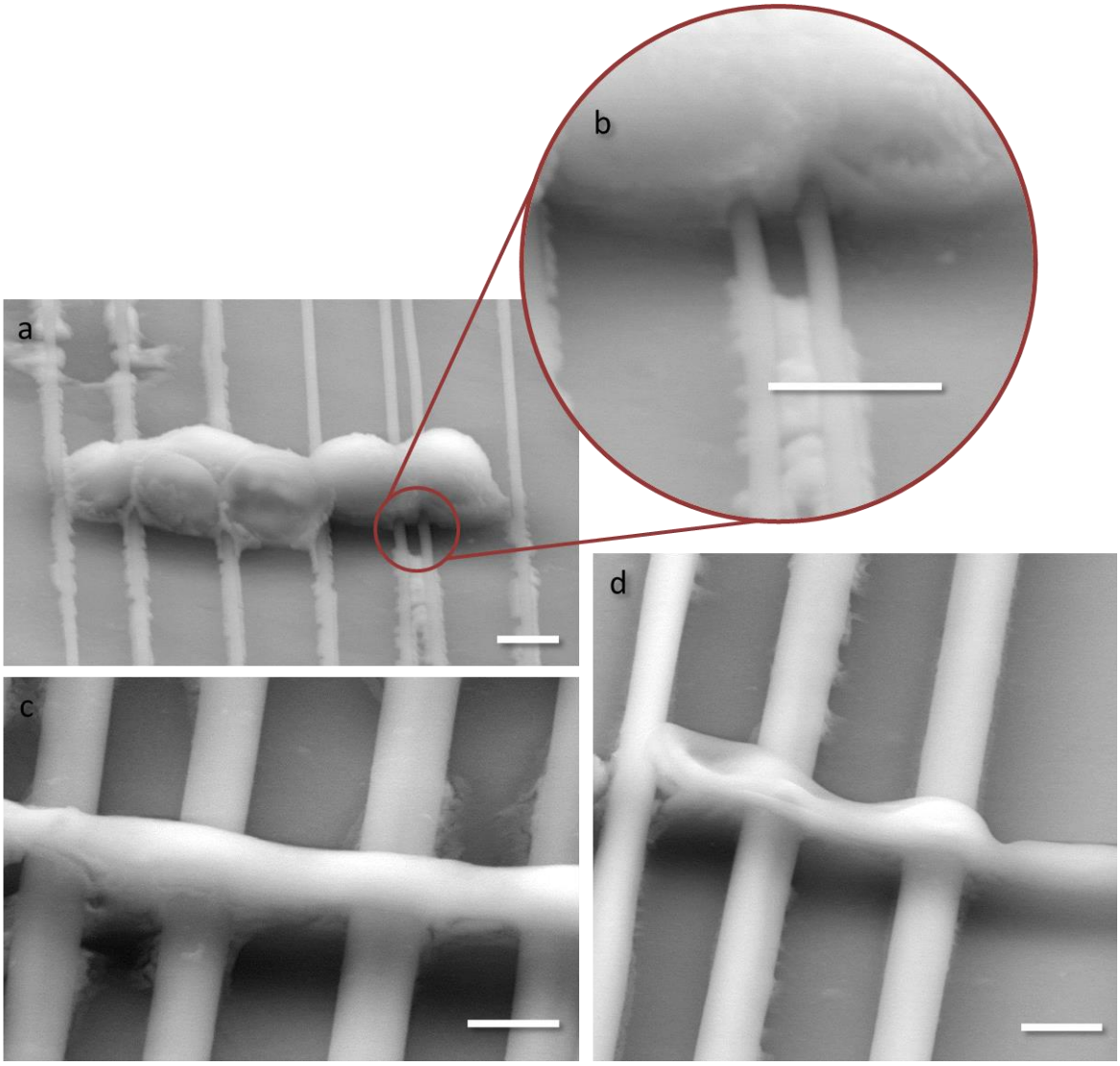

Figure 3.2. The live SEM image of the *C. albicans* was acquired without fixing the cells in order to preserve their natural membrane characteristics. The membrane morphology of the cell adhering to the (a) small diameter (~300 nm) fiber and the (b) zoomed-in image showing deep wrapping of the membrane around the fiber. (c)-(d) On the larger diameter fibers (~1800 nm) the membrane only partial wrapping is observed and cells are not in contact with the underlying substrate. Scale bars represent 2 μm.

3.1.2 Geometric and Volume Constraint

For cell configuration at each diameter, geometrical derivations based on the cross sectional illustration depicted in Figure 3.1 considered. For our cell-nanofiber textured surface interaction model, the cell radius prior to attachment to the surface (R_0), fiber radius (a), and the cell stretching and bending moduli (k_c and k_a) were all knowns. The following are geometric derivations for unknown variables in relation with our known parameters:

$$\delta = (a + \rho)\sin\alpha \tag{3.1}$$

$$\delta = (R - \rho)\sin\beta \tag{3.2}$$

$$R + a - za = (a + \rho)\cos\alpha + (R - \rho)\cos\beta \tag{3.3}$$

Another constraint of the cell shape can be set by the volume conservation of the cell before and after interaction with the fiber written as follows:

$$V_{before} = \frac{4}{3}\pi {R_0}^3 \tag{3.4}$$

$$V_{after} = \frac{4}{3}\pi R^3 - R^3(2\beta - \sin 2\beta) - Ra^2(2\alpha - \sin 2\alpha) + 2R\rho^2(\alpha + \beta - \sin(\alpha + \beta)) \tag{3.5}$$

Using the above geometrical and volume constraints along with equations of energy, the variables were optimized to minimum energy at the state of cell adhesion. The total energy is given by the equation

$$E_{total} = E_{adh} + E_{el} + E_c \tag{3.6}$$

and each component of the energy will be further explained in this chapter.

3.1.3 Adhesion Energy

In the cell attachment process to the nanofiber-textured substrate, the gain in energy arises from the adhesion of the cell membrane to the flat substrate beneath the fiber and/or the nanofibers. This adhesion energy, E_{ad}, is assumed to explain all interactions between cell membrane and the solid substrate, including electrostatic, hydrophobic, and molecular forces (i.e. ligand-receptor bonds). Adhesion energy is explained by:

$$E_{ad} = AS_{ad} \tag{3.7}$$

where A is defined as the adhesion energy density and S_{ad} is defined as the contact area between membrane and surface. The adhesion energy density, A, is a hypothetical constant assumed to encompasses all adhesive interactions the cell has with the surface. The adhesion energy density (A) is assumed to be uniformly distributed around the unperturbed cell membrane. In this work as well as previous work by others [38,39], an initial value of A = 1 erg/cm^2 was used. However we predict this value may be varied for the specific cell type-surface interactions. This cell surface contact area, S_{ad}, highly depends on the degree of penetration, z, which is a function of fiber and cell diameters, as well as the cell moduli of curvature, k_c, and elasticity, k_a. The constant $k_a \approx 200$ dyn/cm^2 is taken from SOPC bilayers [41] but is similar to that of *C. albicans* found using AFM previously [42]. The constant $k_c \approx 1 \times 10^{-13}$erg is also common for SOPC bilayers, although precise measurement of the bending modulus is difficult and based on the method used, it may vary by as much as a factor of 2 [39]. However, it is understood that the bending modulus is typically in the range of few tens of k_BT, as used in this work. We hypothesize that the cell contact area with substrate and fiber will vary with change in fiber diameter (Figure 3.3). Due to the tension caused by the membrane wrapping the fibers, the membrane will eventually lift up from the flat substrate and experience decaying interactions

with the underlying substrate. However, due to the increase in the surface area of the fiber with increasing diameter, the contact area with fiber will increase.

Using simple geometric relations, the contact area of the cell with fiber can be calculated as

$$S_{fiber} = 4a\alpha R \tag{3.8}$$

and the contact area of cell with the underlying substrate can be calculated as

$$S_{sub} = 4R(R - \delta) \tag{3.9}$$

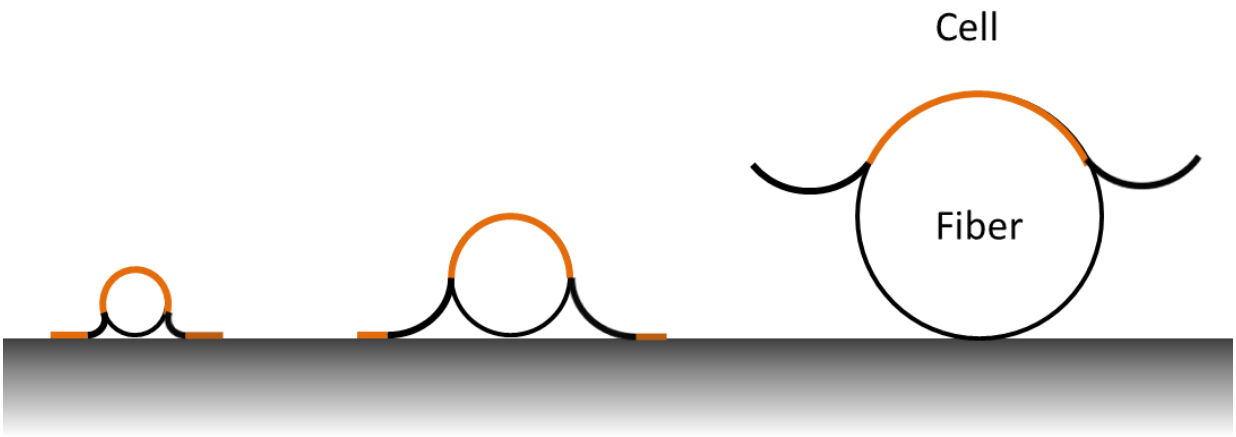

Figure 3.3. The varying ratios of cell radius to fiber radius and the corresponding surface contact area (orange) with substrate and/or fiber. As fiber radius increases, the cell contact area with the substrate decreases while contact area with the fiber increases.

3.1.4 Elastic energy

The main source of loss in energy comes from the deformation of the cell which leads to tension (stretching) and bending of the membrane. Due to the constraint of constant volume for the cell, when the cell adheres to the fiber there is a tension opposing the wrapping of the membrane around the fiber and membrane area must expand. When the membrane is taken as an elastic

sheet with a surface area at rest, or zero tension, to be S_0 and elastic modulus to be k_a, the elastic energy of the membrane can be written as

$$E_{el} = \frac{1}{2} k_a \frac{(S - S_0)^2}{S_0} \tag{3.10}$$

where the difference between the surface area of cell after and before adhesion can be calculated as

$$S - S_0 = 4\pi R^2 + 4aR\alpha - 4\beta R^2 + 2S_T - 4\pi {R_0}^2 \tag{3.11}$$

The surface area of the curvature portion, S_T is as follows:

$$S_T = 2R\rho(\alpha + \beta) \tag{3.12}$$

3.1.5 Net free energies

Another source of energy loss can be seen in the curvature of the membrane, which is naturally resistant to bending. The curvature energy depends on the modulus of curvature, k_c, and is represented by the following equation:

$$E_c = 2k_c \Delta {C_m}^2 \tag{3.13}$$

where $\Delta {C_m}^2$ is the dimensionless value of integrated squared mean curvatures of the final and the initial vesicle. The parameter E_c highly depends on $\sqrt{\frac{k_c}{k_a}}$ which in our case is approximately is only about 10^{-4} fraction of the total energy, therefore can be neglected according to Dietrich [38]. Due to the small value of curvature modulus (k_c = 1×10^{-13} erg), the curvature energy has very insignificant effect on our overall model. However, in cases of cell adhesion to smaller features,

the energies of elasticity and adhesion will diminish, making curvature energy a significant portion of the system.

3.2 Results and Discussions

The change in energy gain from adhesion to fiber and substrate underneath the fiber as a function of the fiber diameter is shown in Figure 3.4a and b, respectively. At the point where the substrate adhesion energy becomes zero, the cell membrane adhered to the substrate comes off the surface due to tension caused by increasing fiber diameter. When the membrane detaches from the surface, some parts of the membrane on fiber also detaches leading to a drop in the fiber adhesion energy as well. However, with increasing fiber diameter, the fiber adhesion energy slowly increases again.

The elastic energy shown in Figure 3.5 indicates that as diameter increases, the elastic energy decreases, meaning more energy is lost with increase in fiber diameter until there is no long adhesion of membrane to the substrate underneath the fiber. The elastic energy loss decreases and eventually reaches near zero as the fiber diameter gets bigger and the radius of curvature decreases.

By summing up the adhesion energies and the elastic energy in the previous figures, we can find the total energy in the process of cell adhesion to the nanofiber-coated substrate. Figure 3.6 shows the sum of all the adhesion energies and elastic energy. We can see that the shape from the model is reminiscent of the trend of the experimental data in Figure 2.6 where the energy starts to decrease then hits a minimum then begin to increase again.

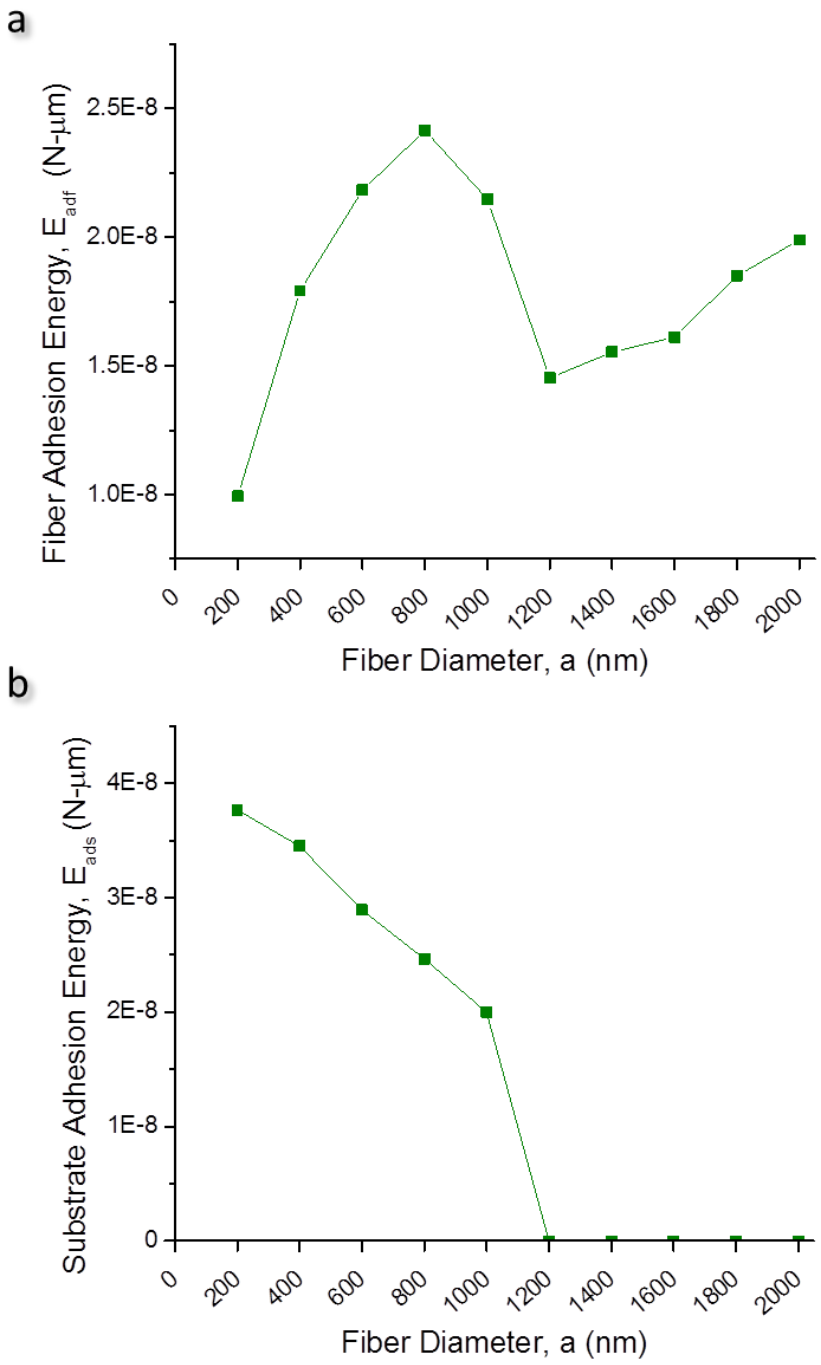

Figure 3.4. Adhesion energy for (a) the cell-fiber interface and (b) the cell-substrate interface as a function of fiber diameter.

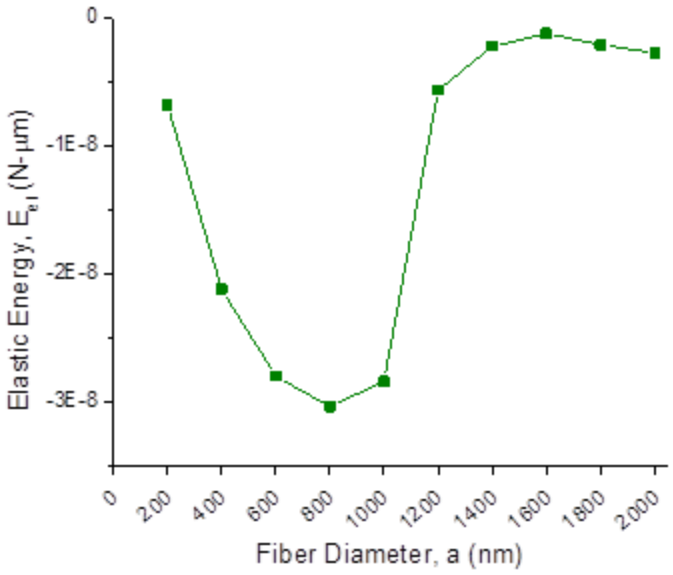

Figure 3.5. The elastic energy due to stretching of the cell is shown as a function of fiber diameter for the nanofiber textured surface. The negative values denote that elastic energy is a loss.

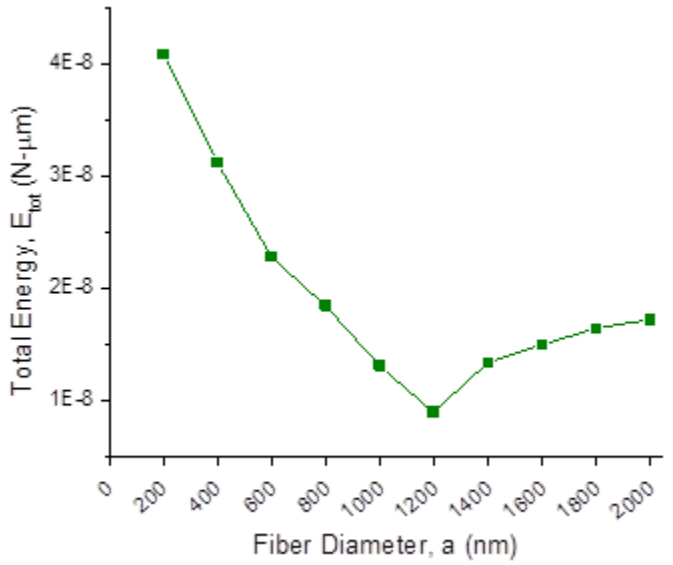

Figure 3.6. The total energy (sum of adhesion energies and elastic energy) is shown as a function of fiber diameter. The "U-shaped" trend supports the experimentally observed trend for population-scale cell attachment density.

3.3 Conclusions

The thermodynamic model, presented herein, describes the adhesion energy associated with the cell adhesion to the fiber and/or the underlying substrate, the elastic energy due to the stretching of the cell, and curvature energy due to the bending of the cell. This model was used to compute the total free energy of a single adherent cell as a function of the fiber diameter for nanofiber-textured surface. We demonstrate that the single adherent cell total free energy trend is similar to the adhesion density trend for the cell population on substrates of different diameters. Our model shows that the energy gain is being lowered as the diameter increases from the lower end until it reached a critical diameter and the energy gain starts to increase again. The high energy gain corresponds to thermodynamic favorability of the cell adhesion to the site. The resemblance of the trend obtained from the model to the result of our experimental data indicates that our single-cell model is a good representation of the population adhesion behavior. We can conclude from our model that it is possible to alter the total energy experienced by cell during the adhesion process solely by varying the surface geometries.

Chapter 4. Discussions and Conclusions

This chapter discusses the experimental analysis and the modeling results from the previous two chapters and summarizes the observations made about cell adhesion to substrates of different topographical feature sizes. Application of our model to *ab initio* design of antifouling materials and other future directions are also discussed. We will conclude with a description of the original contributions of this thesis to the field.

4.1 Discussion of results

Our experimental results for the cell attachment density to nanofiber-textured surface as a function of fiber diameter is supported by the results from the mathematical model for single-cell adhesion, as described in Chapter 3. The "U-shaped" trend shown in Figure 2.6 is explained by the change in adhesion and elastic energies of the membrane as the fiber diameter increases. Due to the decreased energy gain in the cell around the mid-diameter region, it becomes less favorable for the cells to attach to the substrates (Figure 3.4). It can be observed from the live SEM images in Figure 3.2 that the cell membrane takes distinct shape, depending on the topographical feature size of the fibrous substrate. For smaller diameters, the membrane can wrap more deeply around the fiber, having higher z. As fiber diameter increases, the cellular membrane tension is increased, prevent the cell membrane from adhering to the underlying substrate. This allows the penetration z (Figure 4.1) to decrease with the increase in diameter and flatten out towards large fiber diameters where the radius of curvature is small. The decrease in penetration can also be correlated with increasing loss in elastic energy (Figure 3.5). As the tension in membrane increases, it becomes prohibitively expensive for the membrane to wrap around the fiber even though the curvature is decreasing. This will in turn decrease the surface

contact area with the underlying substrate (Figure 3.4b). However, increase in diameter leads to increase in membrane contact area with the fiber, as well as increase the elastic energy, allowing for the total energy to create a "U-shape" (Figure 3.6).

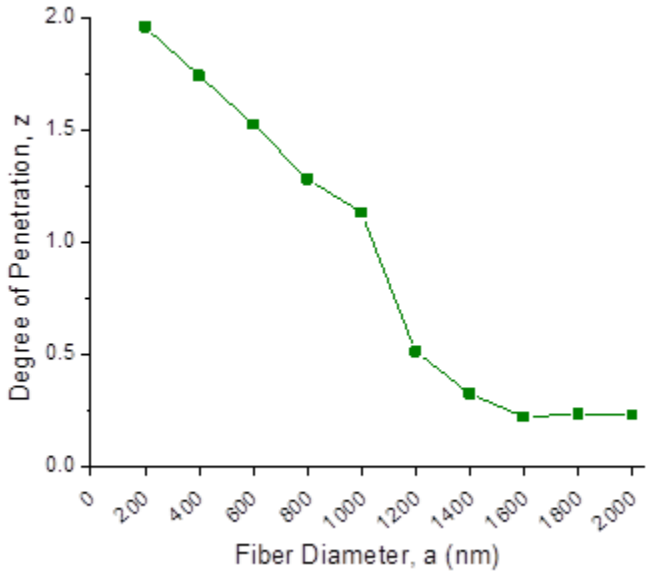

Figure 4.1. The dimensionless degree of penetration, *z*, as a function of fiber diameter, *a*. As fiber diameter increases, the penetration is overall decreasing.

C. albicans take two modes of lifestyle; budding yeast and filamentous hyphae. The spherical yeast cells can have dimensions of 2 to 8 μm in diameter while the hyphal forms typically have 2 μm diameters with large variation in length. Although the morphology of the cell is different, because of the earlier quasi-2D assumption and neglect of edge effects the cross sectional geometry shown in Figure 3.1b can be used to describe the hyphal form as well. However, to take into consideration the elongation of the cell membrane, hyphal length variable is added to the model. When the membrane is interacting with more numbers of fibers, it experiences much higher total energy (Figure 4.2) when compared to that of a spherical cell that is interacting with just a single fiber (Figure 3.6). This could lead to high variations in the cell density for each

diameter range. The hyphal cell also reaches a minimum energy at a lower diameter of ~1000 nm compared to the ~1200 nm with yeast cell. In our experiment, there is a mixture of yeast cells and hyphal cells as shown by the SEM image in Figure 4.5. It is possible that actual model may take a combination of both models, leading to a wide range of minimum density diameters in our experimental data (Figure 2.6).

With the developed model, it is possible to test various scenarios (i.e. different fiber diameters, edge-to-edge spacing, cell diameter, membrane properties) to predict the adhesion density. To verify the feasibility, we tested a case where edge-to-edge spacing is decreased to 1 μm to see its effect on the total energy during the adhesion process. The total energy plot (Figure 4.3) shows that not only did the minimum density diameter shift towards a higher diameter but the magnitude of total energy increases overall. This indicates that 1 μm spacing is more likely to foul compared to 2 μm spacing surface.

Another scenario similar to our catheter experiment in earlier section was conducted by including two separate adhesion density, *A*, in the model for polystyrene fiber and silicone substrate. Because silicone has higher surface energy than polystyrene, the adhesion density was higher for substrate adhesion than that of the fiber adhesion. The total energy of cell adhering to the polystyrene fiber on silicone substrate shown in Figure 4.4 indicate that minimum density is achieved at a much higher fiber diameter compared to the polystyrene fiber-on-polystyrene model in Figure 3.6. This could explain the reason behind a much less reduction of ~1000 nm fibers on silicone catheter compared to the latex catheter which has a similar surface energy compared to polystyrene.

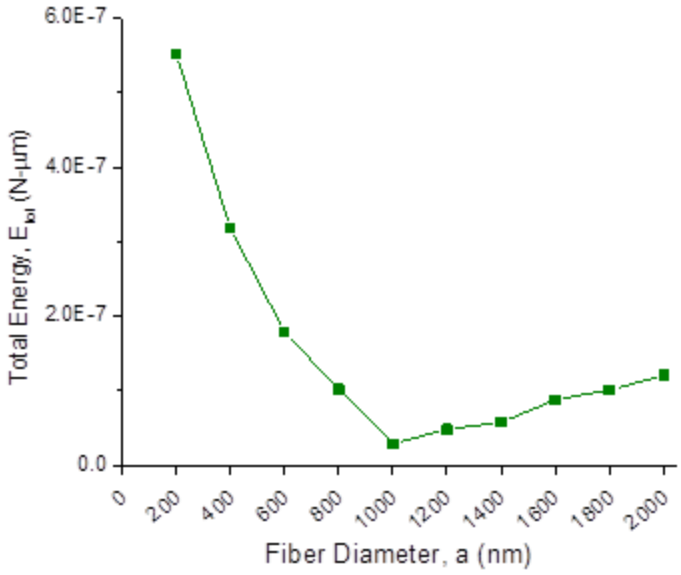

Figure 4.2. The total energy for hyphae with length of 30 μm.

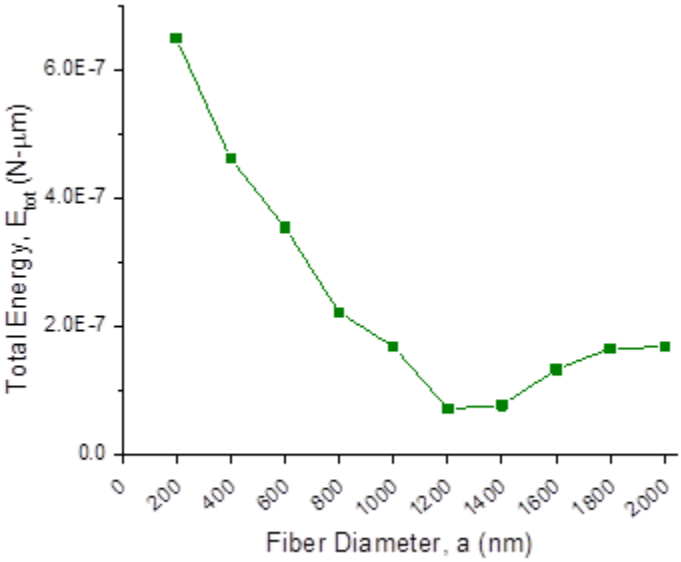

Figure 4.3. The total energy of hyphae with length of 30 μm interacting with surface of fibers with edge-to-edge spacing of 1 μm.

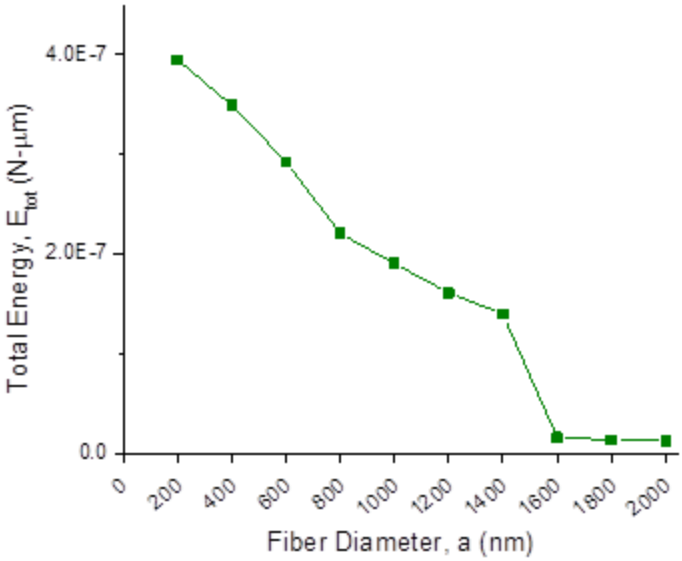

Figure 4.4. The total energy of yeast cell on polystyrene fiber and silicone substrate.

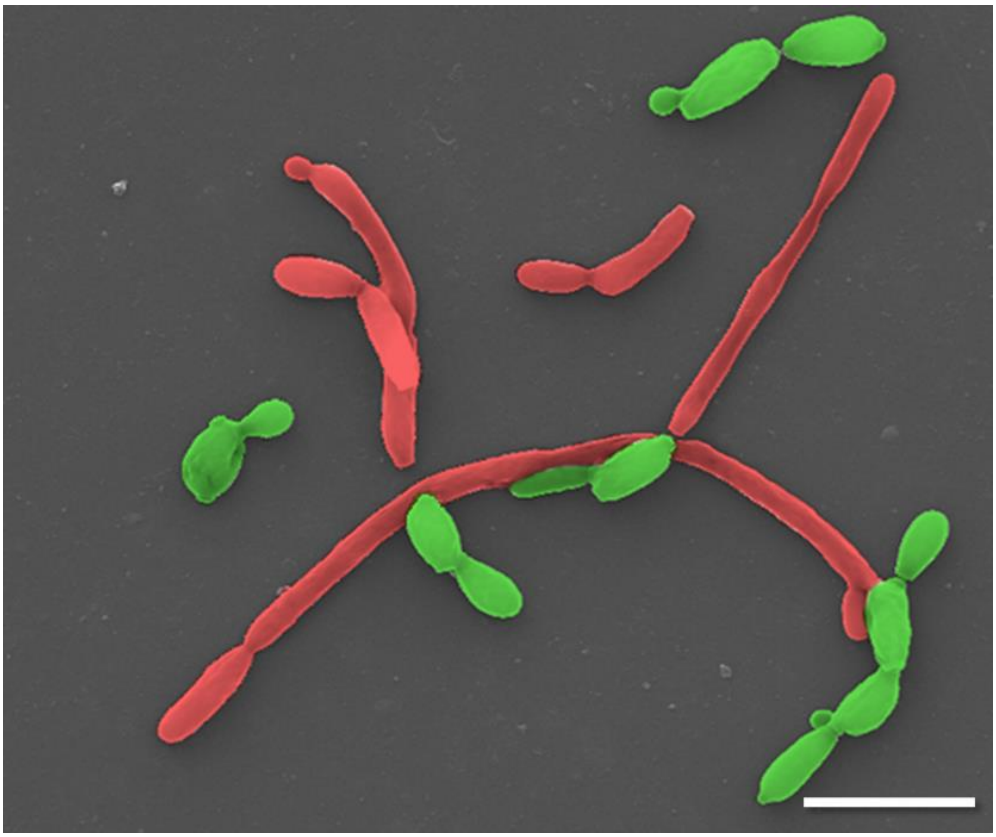

Figure 4.5. The SEM image of *Candida albicans* on bare polystyrene (PS) showing the two lifestyles that the microorganism takes; budding yeast (green) and elongated hyphae (red). The scale bar represents 10μm.

To demonstrate whether the differences between the high and low ends of the "U-trend" are significantly different, statistical analysis was performed by grouping the fiber diameters every 200 nm and averaging the normalized cell numbers within that group. The normalized cell numbers of each group is shown in Figure 4.6 as box plots. The low end groups of 200 – 400 nm and 400 – 600 nm are significantly different from the three mid-diameter groups of 1000 – 1200 nm, 1200 – 1400 nm, and 1400-1600 nm ($p<0.0001$) indicating true decrease in cell adhesion density for the mid-diameter groups compared to the small diameter groups. Similarly, the large diameter groups (1800 – 2000 nm) are significantly different from the three mid-diameter groups ($p<0.001$).

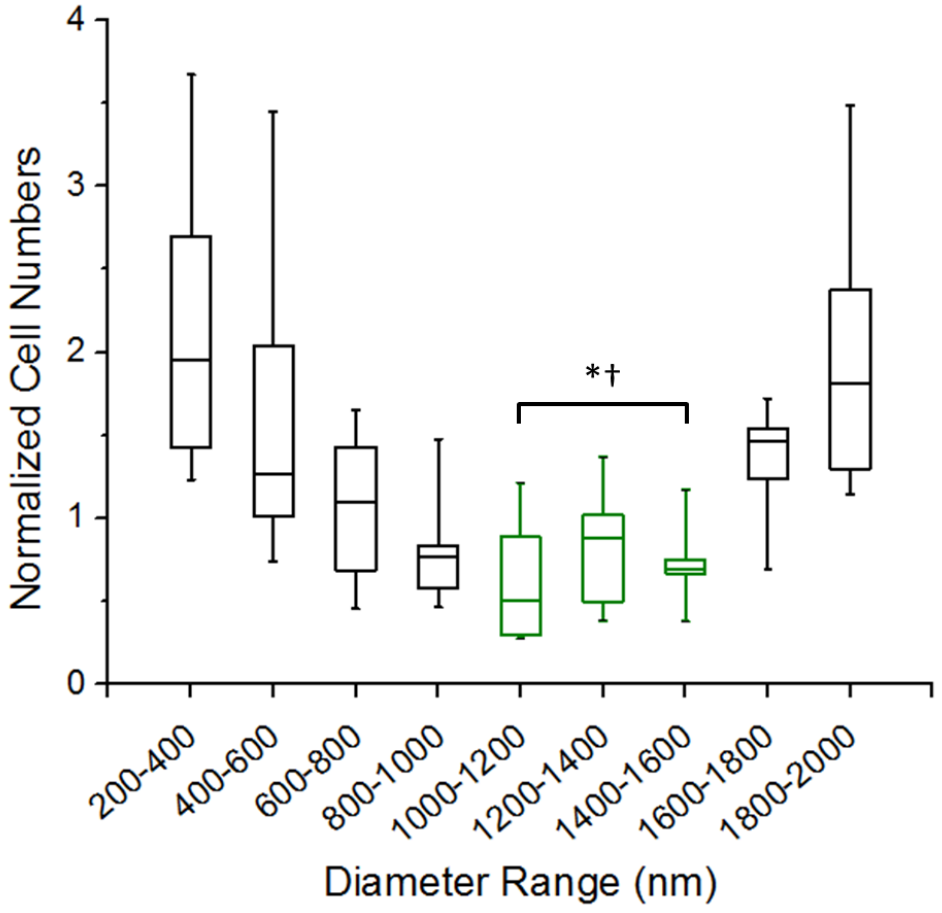

Figure 4.6. The normalized cell numbers are shown as box plots for each diameter range. The ranges where adhesion is minimized (shown in green) is compared to the smallest range (200-400 nm) and largest range (1800-2000 nm) to test significant difference. * $p < 0.0001$ against small diameter (200-400 nm) group. †$p<0.001$ against large diameter (1800-2000 nm) group.

4.2 Summary

This thesis presents a systematic experimental and theoretical investigation of the adhesion of microorganisms to nano-patterned surfaces. To enable this study, highly aligned PS nanofiber coating of controlled diameter and separation distances were deposited on PS surfaces to

determine the effect of a physical stimulus inform of uniform surface roughness, on the adhesion of *C. albicans* cells. Because the underlying substrate is the same material as the nanoscale topographical features, this method does not present any change in chemistry and allows us to probe the effects of physical modification of surface on microorganism adhesion. By fixing the edge-to-edge separation distance between the fibers at 2 μm and varying the fiber diameters from 200 nm to 2000 nm, we were able to arrive at a "U-shaped" trend that has a minimum adhesion at approximately 1000–1400 nm diameters which indicates that purely physical stimuli in form of nanoscale surface topography can increase or reduce cell adhesion depending on the surface feature size. This trend can be explained by the thermodynamic principles of net balance of energy gain and expenditure in the process of adhesion. With deformation due to topographical cues, there will be a certain loss in energy, which will make it thermodynamically less favorable for cells to adhere. This principle is well described by our model in which we summed up the gain in adhesion energy to both the fiber and the underlying substrate and the loss in elastic energy due to deformation and membrane tension. The sum of these energies similarly follows the "U-shaped trend" of the experimental data.

4.3 Significance and contributions

With increasing number of elderly population and consequent increase of indwelling medical devices, medical infection due to biofilm forming microorganism is becoming an increasingly significant challenge. Because of the difficulty in removing biofilm, it is more efficient to devise a method of delay or inhibition of biofilm formation rather than removal. In order to accomplish this, surface needs to be engineered to prevent the adhesion of microorganism. This necessitates the study of adhesion of microorganism on surfaces of different physicochemical properties. Our method allows for the probing of adhesion by simply altering the physical properties. Currently,

this is one of the few, if not only, case of reduction of yeast on surface with sub-micron topographical modifications. Although our study uses simple surface topography modification, the work could be of significant interest to the field because of its versatility as a platform for reducing microorganism adhesion. With the STEP method utilized for fiber deposition, it is possible to alter both the substrate and fiber material. Also, anti-microbial drugs or nanoparticles can be added to the polymeric solution, which can then be spun into fibrous substrates. By studying just the physical effects of diameter on adhesion, we have optimized the topographic features for future works to advance the adhesion delaying properties.

4.4 Future directions

As discussed in Chapter 4, *C. albicans* take multiple forms of life which can change the adhesion behavior to the surface. In addition, we hypothesize that the change in feature sizes may induce changes in the differentiation behavior and phenotype of *C. albicans*. Differentiation is important due to its possible invasive and virulence effects. The effect of feature sizes on the differentiation of the fungal pathogen can be studied further which can also aid in development of the adhesion model.

In previous section, it was discussed that with STEP method, there is a large possibility of alterations of chemical properties of the fibrous substrates. We can extend this research by finding polymers that are more likely to repel adhesion through addition of natural biocides, chemical compounds, surface-modifying end groups (SMEs), nanoparticles, and more.

References

[1] Coenye, T., De Prijck, K., Nailis, H., and Nelis, H. J., 2011, "Prevention of *Candida albicans* biofilm formation," Open Mycol. J., **5**, pp. 9–20.

[2] Costerton, J. W., Lewandowski, Z., Caldwell, D. E., Korber, D. R., and Lappin-Scott, H. M., 1995, "Microbial Biofilms," Annu. Rev. Microbiol., **49**(1), pp. 711–745.

[3] Hawser, S. P., Baillie, G. S., and Douglas, L. J., 1998, "Production of extracellular matrix by *Candida albicans* biofilms.," J. Med. Microbiol., **47**(3), pp. 253–6.

[4] Tacconelli, E., De Angelis, G., Cataldo, M. a, Pozzi, E., and Cauda, R., 2008, "Does antibiotic exposure increase the risk of methicillin-resistant *Staphylococcus aureus* (MRSA) isolation? A systematic review and meta-analysis.," J. Antimicrob. Chemother., **61**(1), pp. 26–38.

[5] Weinstein, R. A., and Darouiche, R. O., 2001, "Device-Associated Infections: A Macroproblem that Starts with Microadherence," Clin. Infect. Dis. , **33** (9), pp. 1567–1572.

[6] Darouiche, R. O., 2004, "Treatment of Infections Associated with Surgical Implants," N. Engl. J. Med., **350**(14), pp. 1422–1429.

[7] Klevens, R. M., Edwards, J. R., Richards, C. L., Horan, T. C., Gaynes, R. P., Pollock, D. A., and Cardo, D. M., 2007, "Estimating Health Care-Associated Infections and Deaths in U.S. Hospitals, 2002," Public Health Rep., **122**(2), pp. 160–166.

[8] Scott, R. D., 2009, "The direct medical costs of healthcare-associated infections in US hospitals and the benefits of prevention."

[9] Hasan, J., Crawford, R. J., and Ivanova, E. P., 2013, "Antibacterial surfaces: the quest for a new generation of biomaterials," Trends Biotechnol., **31**(5), pp. 295–304.

[10] Kirschner, C. M., and Brennan, A. B., 2012, "Bio-Inspired Antifouling Strategies," Annu. Rev. Mater. Res., **42**(1), pp. 211–229.

[11] Campoccia, D., Montanaro, L., and Arciola, C. R., 2013, "A review of the biomaterials technologies for infection-resistant surfaces.," Biomaterials, **34**(34), pp. 8533–54.

[12] Chandra, J., Patel, J., and Li, J., 2005, "Modification of surface properties of biomaterials influences the ability of *Candida albicans* to form biofilms," Appl. Environ. Microbiol., **71**(12), pp. 8795–8801.

[13] Roe, D., Karandikar, B., Bonn-Savage, N., Gibbins, B., and Roullet, J.-B., 2008, "Antimicrobial surface functionalization of plastic catheters by silver nanoparticles.," J. Antimicrob. Chemother., **61**(4), pp. 869–76.

[14] Dror, N., Mandel, M., Hazan, Z., and Lavie, G., 2009, "Advances in microbial biofilm prevention on indwelling medical devices with emphasis on usage of acoustic energy," Sensors, **9**, pp. 2538–2554.

[15] Frade, J. P., and Arthington-Skaggs, B. a, 2011, "Effect of serum and surface characteristics on *Candida albicans* biofilm formation.," Mycoses, **54**(4), pp. e154–62.

[16] Klotz, S. a, Drutz, D. J., and Zajic, J. E., 1985, "Factors governing adherence of *Candida* species to plastic surfaces.," Infect. Immun., **50**(1), pp. 97–101.

[17] Yoshijima, Y., Murakami, K., Kayama, S., Liu, D., Hirota, K., Ichikawa, T., and Miyake, Y., 2010, "Effect of substrate surface hydrophobicity on the adherence of yeast and hyphal *Candida*.," Mycoses, **53**(3), pp. 221–6.

[18] Minagi, S., Miyake, Y., Inagaki, K., Tsuru, H., and Suginaka, H., 1985, "Hydrophobic interaction in *Candida albicans* and *Candida tropicalis* adherence to various denture base resin materials.," Infect. Immun., **47**(1), pp. 11–4.

[19] Radford, D. R., Sweet, S. P., Challacombe, S. J., and Walter, J. D., 1998, "Adherence of *Candida albicans* to denture-base materials with different surface finishes.," J. Dent., **26**(7), pp. 577–83.

[20] Tsang, C. S. P., Ng, H., and McMillan, a S., 2007, "Antifungal susceptibility of *Candida albicans* biofilms on titanium discs with different surface roughness.," Clin. Oral Investig., **11**(4), pp. 361–8.

[21] Verran, J., Lees, G., and Shakespeare, a P., 1991, "The effect of surface roughness on the adhesion of *Candida albicans* to acrylic," Biofouling, **3**(3), pp. 183–191.

[22] Zamperini, C. A., Machado, A. L., Vergani, C. E., Pavarina, A. C., Giampaolo, E. T., and da Cruz, N. C., 2010, "Adherence in vitro of *Candida albicans* to plasma treated acrylic resin. Effect of plasma parameters, surface roughness and salivary pellicle.," Arch. Oral Biol., **55**(10), pp. 763–70.

[23] Liu, K., and Jiang, L., 2011, "Bio-inspired design of multiscale structures for function integration," Nano Today, **6**(2), pp. 155–175.

[24] Crick, C. R., Ismail, S., Pratten, J., and Parkin, I. P., 2011, "An investigation into bacterial attachment to an elastomeric superhydrophobic surface prepared via aerosol assisted deposition," Thin Solid Films, **519**(11), pp. 3722–3727.

[25] Chung, K. K., Schumacher, J. F., Sampson, E. M., Burne, R. a, Antonelli, P. J., and Brennan, A. B., 2007, "Impact of engineered surface microtopography on biofilm formation of *Staphylococcus aureus*.," Biointerphases, **2**(2), pp. 89–94.

[26] Pogodin, S., Hasan, J., Baulin, V. a, Webb, H. K., Truong, V. K., Phong Nguyen, T. H., Boshkovikj, V., Fluke, C. J., Watson, G. S., Watson, J. a, Crawford, R. J., and Ivanova, E. P., 2013, "Biophysical model of bacterial cell interactions with nanopatterned cicada wing surfaces.," Biophys. J., **104**(4), pp. 835–40.

[27] Sudbery, P., Gow, N., and Berman, J., 2004, "The distinct morphogenic states of *Candida albicans*.," Trends Microbiol., **12**(7), pp. 317–24.

[28] Kumamoto, C. A., and Vinces, M. D., 2005, "ALTERNATIVE *CANDIDA ALBICANS* LIFESTYLES: Growth on Surfaces," Annu. Rev. Microbiol., **59**(1), pp. 113–133.

[29] Calderone, R. a, and Fonzi, W. a, 2001, "Virulence factors of *Candida albicans*.," Trends Microbiol., **9**(7), pp. 327–35.

[30] Donlan, R. M., 2001, "Biofilms and device-associated infections.," Emerg. Infect. Dis., **7**(2), pp. 277–281.

[31] Sardi, J. C. O., Scorzoni, L., Bernardi, T., Fusco-Almeida, a M., and Mendes Giannini, M. J. S., 2013, "*Candida* species: current epidemiology, pathogenicity, biofilm formation, natural antifungal products and new therapeutic options.," J. Med. Microbiol., **62**(Pt 1), pp. 10–24.

[32] Seneviratne, C. J., Jin, L., and Samaranayake, L. P., 2008, "Biofilm lifestyle of *Candida*: a mini review.," Oral Dis., **14**(7), pp. 582–90.

[33] Kargar, M., Wang, J., Nain, A. S., and Behkam, B., 2012, "Controlling bacterial adhesion to surfaces using topographical cues: a study of the interaction of *Pseudomonas aeruginosa* with nanofiber-textured surfaces," Soft Matter, **8**(40), p. 10254.

[34] Nain, A. S., Sitti, M., Jacobson, A., Kowalewski, T., and Amon, C., 2009, "Dry Spinning Based Spinneret Based Tunable Engineered Parameters (STEP) Technique for Controlled and Aligned Deposition of Polymeric Nanofibers," Macromol. Rapid Commun., **30**(16), pp. 1406–1412.

[35] Chandra, J., Mukherjee, P. K., and Ghannoum, M. A., 2008, "In vitro growth and analysis of *Candida* biofilms," Nat. Protoc., **3**(12), pp. 1909–1924.

[36] Honraet, K., Goetghebeur, E., and Nelis, H. J., 2005, "Comparison of three assays for the quantification of *Candida* biomass in suspension and CDC reactor grown biofilms.," J. Microbiol. Methods, **63**(3), pp. 287–95.

[37] Scardino, A. J., Guenther, J., and de Nys, R., 2007, "Attachment point theory revisited: the fouling response to a microtextured matrix," Biofouling, **24**(1), pp. 45–53.

[38] Dietrich, C., Angelova, M., and Pouligny, B., 1997, "Adhesion of Latex Spheres to Giant Phospholipid Vesicles: Statics and Dynamics," J. Phys. II Fr., **7**(11), pp. 1651–1682.

[39] Deserno, M., and Gelbart, W. M., 2002, "Adhesion and Wrapping in Colloid−Vesicle Complexes," J. Phys. Chem. B, **106**(21), pp. 5543–5552.

[40] Shao, Y., and Fu, J., 2014, "Integrated micro/nanoengineered functional biomaterials for cell mechanics and mechanobiology: a materials perspective.," Adv. Mater., **26**(10), pp. 1494–533.

[41] Evans, E., and Needham, D., 1987, "Physical properties of surfactant bilayer membranes: thermal transitions, elasticity, rigidity, cohesion and colloidal interactions," J. Phys. Chem., **91**(16), pp. 4219–4228.

[42] Kim, K. S., Kim, Y.-S., Han, I., Kim, M.-H., Jung, M. H., and Park, H.-K., 2011, "Quantitative and qualitative analyses of the cell death process in *Candida albicans* treated by antifungal agents.," PLoS One, **6**(12), p. e28176.